Project Title: Ocean and Sea Ice and their Interactions around Greenland and the West Antarctic Peninsula in Forced Fine-Resolution Global Simulations

Federal Award Identification Number: DE-SC0014378

Agency Code: 8900

Organization: Office of Biological & Environmental Research

Project Period: 08/01/2015 - 07/31/2018

Principal Investigator Information:
Prof. Eric Chassignet
Center for Ocean-Atmospheric Prediction Studies
2000 Levy Avenue
Tallahassee, FL 32306-2741
Email: echassignet@fsu.edu
Contact: (850) 645-7288

FINAL REPORT

1. What are the major goals of the project?

The overarching science objective of the project is to use a series of forced global high resolution numerical simulations based on two ocean general circulation models (OGCMs), each coupled to a thermodynamic/dynamic ice model, to investigate how the interplay of regional processes and decadal changes in local and remote forcing impact the delivery and end member composition of waters over the continental shelves of Greenland and Antarctica. Anomalously warm ocean waters have been implicated as the cause of accelerated ablation along the margin of the Greenland ice sheet, as well as the cause of increasing basal melt rate, mass loss, and grounding line retreat of many Antarctic ice shelves. Specifically, we consider the waters at the mouths of the Greenland fjords and those over the continental shelves in the vicinity of the mouths of ice cavities in Antarctica. To meet our objective, our study needs to be of sufficient length to resolve decadal variability and to capture the changes to the Southern Annular Mode (SAM) in the Southern Ocean, the El Niño Southern Oscillation (ENSO), the North Atlantic Oscillation (NAO), and the Atlantic Multidecadal Oscillation (MAO) in the tropical and midlatitude North Atlantic over the last 50 years. In addition, the realistic delivery of anomalous water masses over the continental and slope will require the explicit resolution of small scale (~5 km) eddies, fronts, and meanders. To overcome this dichotomy of scales and meet our objective, we proposed to use a series of forced global ocean/sea ice simulations that first focus on decadal, basin scales processes and then later on smaller scale processes in shorter duration simulations using ultrahigh horizontal meshes.

Our specific project goals were to:

1) Understand how changes and variability in the ocean basins surrounding Greenland and Antarctica affect the composition of the water masses reaching the continental shelf waters of these land masses from 1960-2009. In the case of Greenland, we need to consider

upstream conditions in the Arctic and in the North Atlantic, especially the changing Arctic sea ice cover. In the Antarctic, our focus will be on west Antarctica where the largest basal melt rates have been reported, particularly the Amundsen Sea which in downstream of the Pine Island Glacier. We will use an existing 60-year 0.1° global coupled ocean/sea ice (POP/CICE) simulation that was forced with Coordinated Ocean Reference Experiment-II interannually varying forcing (CORE-II IAF) atmospheric fluxes for 1948-2009; the simulation is mesoscale eddy resolving equatorward of 50° N/S.

2) Setup and run a new global tripole configuration of POP grid with ultrahigh resolution around Greenland and the Antarctic continent. The horizontal resolution will be roughly 23 km resolution over the southeast and west Greenland continental shelf/slope and, in the Southern Hemisphere, between 1°-2° in the Amundsen Sea and 2°-3° over the west Antarctic Peninsula. Such ultrahigh resolution should explicitly resolve ~5-6km scale eddies and meanders in both study regions, as well as continuing to resolve mesoscale eddies in the tropical and midlatitude oceans. Like (1) it will be forced with CORE-II IAF. It will be run for several decades to demonstrate the importance of resolving very small scale mesoscale features and mixing processes over these continental shelves.

3) Configure and run regional Arctic Cap 1/25° and 1/50° Hybrid Coordinate Ocean Model (HYCOM)/CICE models forced with interannual forcing. HYCOM uses a hybrid vertical coordinate system that is terrain following near the continental slope/shelf, isopycnal in the interior, and has pressure levels in the mixed layer and unstratified seas. Again, the processes responsible for changes and variability in the delivery and end member composition of the water masses over the Greenland shelf will be examined. As well, existing global 1/12° HYCOM/CICE results will be analyzed in the Northern high latitudes. The robustness of the processes responsible for the anomalous high latitude warming in POP and HYCOM models will be challenged and verified by using different ocean models together with available observations.

2. What was accomplished under these goals?

Goal 1 and 2: See partner report from McClean (SIO)
Goal 3: HYCOM Arctic Cap simulations

Presentations at scientific meetings and workshops, seminars:

Dukhovskoy, D.S., E. Chassignet, L. Stefanova, O-M. SMedstad, J. Metzger, P. Posey, A. Wallcraft, “Current State and Recent Changes in the Arctic Ocean from the HYCOM-NCODA Global Ocean and Sea Ice Prediction System”, AGU Fall, 2016, oral.

Dukhovskoy, D.S. and E. Chassignet, “Role of Greenland fresh water in the Arctic climate system: An insight from the HYbrid Coordinate Ocean Model experiments”, DOE 2016 Regional and Global Climate Modeling (RGCM) PI Meeting, 2016, poster.

Dukhovskoy, D.S., “Freshwater pathways in the Arctic Ocean and North Atlantic from numerical experiments with passive tracers”, FAMOS workshop, WHOI, 2017, oral.

Dukhovskoy, D.S., “The role of fresh water in a changing Arctic climate”, IARPC seminar, 2018, oral.

Dukhovskoy, D.S., “Freshwater fluxes in the Arctic Ocean – North Atlantic climate system”, NOAA AOML seminar, 2018, oral.

Dukhovskoy, D.S., "Freshwater fluxes in the Arctic Ocean – North Atlantic climate system", Saint-Petersburg State University, seminar, 2018, oral.

Dukhovskoy, D.S., "Pathways of Greenland fresh water in coastal regions", Estuarine and Coastal Modeling Conference, 2018, oral.

Dukhovskoy, D.S., A. Proshutinsky, M. Bourassa, "Wind-driven freshwater fluxes in the Arctic Ocean and Subarctic seas", EGU, 2018, oral.

Dukhovskoy, D.S., "Fresh water in a changing Arctic", LANL, 2018, seminar.

Dukhovskoy, D.S., "Influence of Greenland fresh water on salinity of the Subpolar North Atlantic", Naval Postgraduate School, 2018, seminar.

Dukhovskoy, D.S., and E. Chassignet, 2018, "Freshwater pathways in the Arctic Ocean and Northern North Atlantic from a numerical experiment with passive tracers", Ocean Sciences Meeting, 2018, poster.

Dukhovskoy, D.S., "Greenland fresh water in the subpolar North Atlantic", LANL, 2019, seminar.

Publication:

D.S. Dukhovskoy, I. Yashayaev, A. Proshutinsky, J.L. Bamber, I.L. Bashmachnikov, E.P. Chassignet, C.M. Lee, and A.J. Tedstone, 2019: Role of Greenland Freshwater Anomaly in the Recent Freshening of the Subpolar North Atlantic, JGR, in revision.

In order to investigate the impact of high resolution on multi -decadal simulations of the Greenland shelf waters, we configured and run coupled 0.08° and 0.04° regional Arctic Ocean HYCOM and CICE model (Figure 1) to study both mesoscale and submesoscale processes involved in frontal mixing over the Greenland shelf, as well as changes to the water masses there over multiple decades.

The main objective of the first experiment (0.08°) is to track pathways and fate of Greenland fresh water as well as propagation and spreading of fresh water from the Arctic Ocean, particularly over the Greenland shelf and adjacent basins. Several improvements to the model setup in this application are made compared to the experiment presented in Dukhovskoy et al. (2016). First, the present model configuration uses improved bathymetry with shallower coastline (5 m as compared to 10 m in the old configuration). Second, in the current configuration, HYCOM employs a vertical grid with more vertical layers (41 compared to 32 in the old configuration) that provide higher resolution in the upper 1500 m. Third, the model experiments are integrated for a longer period of time, from 1993 through 2016, which is the time period that covers the duration of the accelerated Greenland ice sheet melt (Bamber et al., 2012; 2018). Next, the simulations are driven by continuous atmospheric forcing, Greenland freshwater flux, and more realistic ocean fields imposed at the lateral open boundaries. The 0.08° AO-HYCOM is nested within the 0.08º Global HYCOM + NCODA GOFS3.0 reanalysis (Metzger et al., 2014) (for 1993–2005) and GOFS3.1 analysis (2006–2016), which provide more realistic ocean fields at the lateral open boundaries. The ocean forcing fields are derived from the daily reanalysis and analysis fields at seven-day frequency providing realistic lateral fluxes of salt, heat, and mass across the boundaries. No salinity restoring is applied in the experiments. Atmospheric fields are obtained from the National Centers for Environmental Prediction (NCEP) Climate Forecast System Reanalysis (CFSR) (Saha et al., 2010) for 1993–2011 and CFSv2 (Saha et al., 2014) for 2012–2016. And finally, the experiment in this study is 10 years longer than the experiment in Dukhovskoy et al. (2016). The duration of the previous model experiment was not long enough to analyze the Greenland freshwater anomaly

(GFWA) pathways in all basins. Sea ice was initialized in January 1, 1993 from the PIOMAS sea ice reanalysis.

The high-resolution 0.04° configuration uses the Digital Bathymetric Data Base Variable Resolution (DBDB-V2) from the U.S. Naval Oceanographic Office (NAVOCEANO) "T17" prepared by the Navy Research Laboratory at the Stennis Space Center with some changes. Specifically, the Fury and Hecla Strait was opened in the model topography (which is closed in the original topography T17). This strait is the only direct connection of Hudson Bay with the Arctic Ocean and it plays an important role in the local freshwater and heat exchange between the basins.

For both model configurations, there are twin experiments performed with and without the Greenland freshwater flux imposed along the coast. The 0.08 HYCOM-CICE experiments are initialized from a spin-up simulation started from the ocean climatology fields from the Generalized Digital Environmental Model version 4 (GDEM4) and are integrated for 1993–2016. One experiment is conducted without any freshwater flux from Greenland (hereinafter referenced as "GR–"). In the other experiment, the total freshwater flux is imposed at the freshwater sources along the coast of Greenland from the beginning of the simulation ("GR+"). Locations and magnitudes of the Greenland freshwater fluxes are prescribed based on Bamber et al. (2012; 2018). The data are a monthly gridded product (5 × 5 km grid) with realistic geographic distribution and temporal variability (Figure 2). Greenland runoff was derived from a reconstruction of the surface mass balance of the Greenland Ice Sheet and surrounding tundra using a high-resolution regional climate model, RACMO2 forced with ERA-40 re-analysis data. The runoff from the ice sheet and surrounding tundra was combined with observations of solid ice discharge derived from satellite observations of ice velocity to produce the total freshwater flux to the ocean. The Greenland freshwater flux for the model experiments is obtained from the first data set of Bamber et al. (2012) until 2010 and from the second data set of (Bamber et al., 2018) for 2011–2016.

In order to track the fresh water from different sources and assess their impact on thermohaline changes in the Arctic Ocean and North Atlantic, passive tracers are continuously released at the specified locations (Figures 2 and 3). There are 5 passive tracers tracking (1) Greenland freshwater, (2) Mackenzie River, (3) Eastern Eurasian rivers (east of the Kara Sea), (4) western Eurasian rivers (west of the Kara Sea including it), (5) Pacific water in the Bering Strait. The tracer fluxes are set proportional to the freshwater fluxes of the selected sources. In HYCOM, runoff from a single source is distributed over several grid cells. Similarly, the passive tracer is continuously released in the upper 6 m at the same model grid cells that has nonzero river runoff. The tracer is prescribed in the model by relaxing tracer concentration in the specified locations, which are ocean grid cells nearest to the freshwater sources along the Arctic and Greenland coastlines, to the maximum concentration value that is defined as follows.

For the given Greenland (or Arctic river) freshwater flux (F_{Gr}, $m^3\ s^{-1}$) at some location ($\mathbf{x}$), the tracer concentration ($kg\ m^{-3}$) is defined as

$$C_{tr}(\mathbf{x},t) = \frac{\alpha \cdot F_{Gr}(\mathbf{x},t) \cdot t_{rlx}}{v(\mathbf{x},t)}, \quad (1)$$

where t_{rlx} is tracer relaxation time scale (one day, here) and $v(\mathbf{x}, t)$ is a grid cell volume (m^3), which is generally a time-dependent quantity in HYCOM; α is a coefficient of proportionality that relates the tracer mass (m_{tr}) to the volume of GFWA accumulated in a grid cell ($v_{Gr}(\mathbf{x})$)

$$m_{tr}(\mathbf{x}, t) = \alpha \cdot v_{Gr}(\mathbf{x}, t). \quad (2)$$

In (1), α is taken to be 1000 for creating forcing fields of C_{tr} for the simulations. The coefficient can be viewed as tracer "density," as it has units (kg m^{-3}). It should be kept in mind that α is merely a proportionality coefficient that can be changed to any value in order to scale the tracer concentration to different values of F_{Gr} if needed, and it does not have any impact on the tracer advection or diffusion in the model.

A passive tracer is advected and mixed similar to other scalar fields using the same advection-diffusion equations and turbulence algorithms. In the present experiments, tracers and scalars are advected using a second-order Flux Corrected Transport (Bleck and Benjamin, 1993; Bleck, 1998). Horizontal diffusivity is numerically formulated as

$$\nu \frac{\partial S}{\partial x} = u_d \delta S, \quad (3)$$

where δS is a salinity (or tracer) difference between the two adjacent grid cells, and $u_d \equiv \frac{\nu}{\Delta x}$ is a diffusion velocity (Bleck et al., 1992), the value for which is given in Table 2.

In the current simulation, the interior ocean mixing is simulated using the K-Profile Parameterization (KPP, Large et al., 1994) vertical mixing algorithm (Wallcraft et al., 2009). Contributions of resolved shear instability, unresolved shear instability due to the background internal wave field, and double diffusion are added to the coefficient of the interior diffusivity. Convective overturning is approximated by the KPP vertical mixing parameterization by specifying high diffusivity in convectively unstable regions. Under a convective regime, the scalar turbulent velocity scale is estimated based on the convective velocity scale

$$w^* = -\left(\frac{B_f}{h}\right)^{\frac{1}{3}}, \quad (4)$$

where B_f is the surface buoyancy flux and h is the surface boundary layer thickness.

At the lateral open boundaries, HYCOM is forced by the oceanic fields derived from the HYCOM+NCODA Global 0.08° Reanalysis (GLBb0.08). GLBb0.08 reanalysis has different topography and vertical hybrid grid compared to the 0.08° and 0.04° AO HYCOM (Figures 3 and 4). For doing this, an automated multi-step nesting algorithm has been developed that prepares nest fields to force HYCOM at the open boundaries. The model experiment is integrated from 1993 to 2015 and just finished 2014.

Model performance and intercomparison of 0.08° and 0.04° HYCOM-CICE

0.08° HYCOM-CICE has been validated against climatological fields, satellite and in situ observations. Validation of the 0.04 simulations and comparison between the 0.04° and the 0.08° simulations is in progress. Some results of the model assessment and model intercomparison are presented below.

Circulation and EKE in the 0.08° and 0.04°

Both models realistically represent mesoscale circulation in the region with the major currents in terms of their location and magnitudes (Figure 4). The boundary currents around Greenland (East Greenland Current, West Greenland Current, and the Labrador Current) are of particular importance of the studied problem. Employing the higher-resolution configuration (0.04) does not provide any obvious benefits for more accurate representation of the mesoscale circulation. For example, both models represent a 3-core structure of the flow on the southeastern Greenland shelf (bottom Figure 4) with the Irminger Current at the offshore position, East Greenland Current (EGC) and the East Greenland Coastal Current (EGCC). This result is not surprising, however, because the spatial scales of the mesoscale mean circulation are well resolved in the 0.08° HYCOM-CICE. The differences are more noticeable in the eddy fields between the two simulations. Mean eddy kinetic energy (EKE) fields show higher eddy energy in the 0.04° HYCOM-CICE compared to the 0.08 simulation (Figure 5). The spatial pattern of the mean EKE has a good general agreement with available estimates derived from drifters and satellite observations showing maximum EKE in the Gulf Stream, near the southern Greenland shelf, and in the eastern Nordic Seas (Richardson, 1983; Heywood et al., 1994; Jakobsen et al., 2003). Note a local maximum of the EKE in the Denmark Strait discussed in (Havik et al., 2017).

Impact of the horizontal resolution on eddying regime in the simulations is apparent from figure 6 presenting vorticity of the 100-m velocity fields normalized by the Coriolis parameter in the Nordic Seas. In the 0.08° HYCOM-CICE, there are markedly fewer eddies compared to the 0.04° HYCOM-CICE suggesting weaker lateral advection of water masses across the boundary current fronts into the interior domain.

The higher-resolution simulation has a better representation of the coastal jets and currents over the Greenland shelf that have small horizontal spatial scales (Bacon et al., 2014; Le Bras et al., 2018) requiring high resolution in the models that are able to resolve the trapping scale of the coastal currents and jets. The East Greenland Coastal Current (EGCC) in the 0.04 HYCOM-CICE is narrow and closely follows the coast line (in agreement with Bacon et al., 2014), whereas the EGCC is more disperse and spreads over most of the shelf as depicted in the 100-m T field in figure 7. The Irminger current is stronger and warmer in the 0.04° HYCOM-CICE compared to the 0.08° HYCOM-CICE, carrying more heat to the northern Labrador Sea and to the Labrador Current. The eddies in the Northerm Labardor Sea are well observed in the temperature field from the 0.04° HYCOM-CICE, whereas there are less eddies in the 0.08° HYCOM-CICE simulation. The eddies are more obvious in the velocity fields shown in figure 8.

Impact of the Greenland freshwater flux on salinity fields in the adjacent regions

The numerical experiments with the 0.08° and 0.04° HYCOM-CICE clearly demonstrate importance of the Greenland freshwater flux for salinity fields not only in the coastal and shelf regions but also in the far offshore areas. As an illustration, Figures 6 and 7 show summer (JJA) mean surface S fields in the two model experiments and 0.08 Global HYCOM+NCODA Reanalysis. In both simulations, S field in the coastal areas of Greenland is markedly fresher (>2) than S fields in the reanalysis and even in more remote locations, Baffian Bay and western Greenland and Irminger seas, surface salinity is less saline (by > 1) than reanalysis. Strong positive

bias in the reanalysis fields is explained by the absence of observational data that could be assimilated. At the same time, 0.08° Global HYCOM reanalysis does not include Greenland freshwater fluxes.

Freshwater and volume fluxes on the Greenland shelf and major straits

In order to assess the reliability of the model performance, freshwater and volume fluxes are calculated across Fram Strait, Denmark Strait, Davis Strait, Nares Strait and the southeast shelf section (figure 11) and compared to the observed-derived estimates reported in the previous studies (Table 1). Presented in figure 12 are estimates from the 0.08° HYCOM-CICE. The 0.04° HYCOM-CICE output are analyzed. All volume transports (figure 12b) have a good agreement with the reported observations. Freshwater transports (figure 12a, note different reference S in some observations listed in Table 1) are also in agreement with observations except for Nares Strait, where the reported freshwater transport estimate was derived based on only a few observations conducted in early August 2003. The model realistically represents seasonality in the freshwater transport discussed in previous studies (Vage et al., 2013; de Steur et al., 2017; Le Bras et al., 2018).

Freshwater fluxes across the Greenland shelf derived from the tracer analysis

In order to analyze the shelf-basin freshwater and heat fluxes, the tracer flux is calculated across a closed contour ($\partial\mathbf{\Omega}$) around Greenland that generally follows the 800-m isobath (figure 13a). The total net flux across the contour is

$$F(t) = \int_{D_b(\mathbf{x})}^{0} \int_{\partial\Omega} C_{tr}(\mathbf{x},t)\mathbf{u}(\mathbf{x},t)\cdot\mathbf{n}\, dl\, dz, \qquad (5)$$

where D_b is the local bottom depth, C_{tr} is tracer concentration (kg m^{-3}) and $\mathbf{n}$ is a normal vector directed towards Greenland.

The mean Greenland tracer flux is normalized by the total net flux (Eq. (5)) yielding the fraction of the total depth-integrated tracer flux along the contour (Figure 13). As expected, the mean net flux for 2000–2016 is strongly negative (i.e., the tracer is fluxed out of the contour), with the strongest tracer outflow across the southwest and south segments of the contour, in good agreement with results from another tracer study by Luo et al. (2016). The northeastern part of the contour has the smallest magnitude of the tracer flux suggesting minimal spreading of GFWA across the East Greenland Current to the interior Nordic Seas. The currents rapidly advect the tracer distributed by the individual sources along the eastern and southern coast towards the southwestern Greenland shelf where the major shelf-basin flux of GFWA occurs. The tracer shelf-basin flux analysis suggests that 85% of the annual depth-integrated GFWA from the shelf to the ocean occurs across the southwestern Greenland continental shelf break between the Davis Strait and Cape Farewell (Figure 13b). The seasonal signal is quite small over most of the contour and is more noticeable over the southwestern segment. Seasonality is more strongly pronounced in the fluxes integrated over the upper 50 m (Figure 13c) compared to the whole depth-integrated fluxes (Figure 13c). In general, the outflow is higher during winter. The interannual variability depicted by the 10th and the 90th percentiles (grey lines in Figures 13b and 13c) has the strongest signals over the southwestern segment of the contour. Again, the near-surface fluxes exhibit stronger

signal than the full depth-integrated fluxes. The obvious disparity in the amplitude of temporal variability in the near-surface and full-depth fluxes suggests that this variability can be primarily driven by wind forcing. To test this idea, a simple regression is fitted to the data

$$Q(t) = \alpha + \beta u_{10}(t), \quad (6)$$

where Q is anomalies of the monthly mean tracer flux averaged between 2000 and 3800 km segment (Figure 13a), u_{10} is the CFSR and CFSv2 10-m wind vector projected onto the 800-m isobath such that negative projection corresponds the upwelling-favorable wind direction in this region. Monthly climatology is removed from both fluxes and winds prior the analysis. The regression has a good fit to data (p-value of the overall F-test is $<1\text{x}10^{-12}$, $\alpha=0$, $\beta=7.6\text{x}10^{-3}$ and $8.4\text{x}10^{-3}$ for the 50 m and full-depth fluxes, respectively). Compared to the full-depth fluxes, the relationship between the wind and the flux anomalies is much stronger for the near-surface fluxes. The regression explains 67% of the variability in the near-surface fluxes versus only 45% for the full-depth fluxes.

Inspection of the monthly mean fluxes integrated over the whole depth (Figures 13b and 13c) versus the fluxes integrated over the upper 50 meters (Figure 13c) reveals relatively homogeneous vertical distribution of the tracer in the water column. The contribution of the subsurface flux (below 50 m) to the total tracer flux is greater than the contribution of the near-surface flux, despite the fact that the Greenland tracer is released in the model surface layers. This result suggests that the tracer (as well as Greenland fresh water) undergoes intense vertical mixing as it travels across the shelf.

Mean and eddy heat fluxes across the Greenland shelf

Mean and eddy heat fluxes (reference T=0° C) across the Greenland contour are calculated from 0.08° HYCOM-CICE (Figure 14). Following the usual approach, the fluxes are decomposed into the time mean and time-fluctuating (eddy) components. The reference time averaging period is 1 month. The model shows that the magnitude of the mean heat flux is several times bigger than the eddy heat flux. The mean eddy heat flux is nearly homogeneously directed towards Greenland, whereas the mean heat flux is more variable across the contour. Most of the heat flux exchange between the Greenland shelf and the deep basins occur across the southwestern–southeastern segment of the contour, similar to the freshwater fluxes.

Vertical mixing of Greenland fresh water on the Greenland shelf

Two mechanisms possibly responsible for the intensified vertical mixing of fresh water on the Greenland shelf are investigated using 0.08° HYCOM-CICE. One is vertical mixing driven by strong along-coastal winds dominating the Greenland shelf. The other is convection during the cold season on the western Greenland shelf (discussed in Marson et al., 2017). Here, vertical spreading of the passive tracer on the Greenland shelf and deep ocean is analyzed to demonstrate vertical distribution of the Greenland fresh water in the water column simulated in the 0.08 HYCOM-CICE.

Several previous studies discuss an “Ekman straining” mechanism that impacts the horizontal and vertical scales and mixing of the buoyant coastal currents (e.g. Fong and Geyer, 2001). During downwelling favorable winds, the current is confined against the coast becoming narrower and

thicker with enhanced vertical salt flux. In contrast, during upwelling favorable winds the current spreads off shore and becomes thinner and even more susceptible to vertical mixing of salt. In this study, winter (October–March) and summer (April–September) wind statistics derived from the CFSR and CFSv2 surface wind fields are analyzed for several locations along the coast of Greenland (black bullets in Figure 15a). From the wind roses presented in 15 it follows that north winds are the most frequent and strongest over the east Greenland shelf. The central and southern parts of the west Greenland shelf are dominated by north winds in winter, whereas the north and south winds are nearly equal in frequency and strength during summer. North winds are downwelling-favorable for the east coast of Greenland and upwelling-favorable for the west coast. North winds push surface water towards the coast, thus precluding Greenland fresh water (and the tracer) to move offshore. In contrast, north winds over the west Greenland shelf facilitate the offshore spreading of Greenland fresh water (and the tracer) in the Ekman layer. The CFSR and CFSv2 wind fields are used to estimate wind-driven upwelling and downwelling processes along the coast of Greenland. The Ekman transport is calculated from the surface wind stress providing winter and summer upwelling indices shown in figure 15a and 15b. The Ekman transport vector is projected onto a vector aligned with the bathymetric gradient, positive toward deeper water. Thus, the index is the Ekman transport in the offshore direction (m^3 s^{-1} per 1 m of the coast line), i.e. a negative transport corresponds to downwelling.

The locations and seasonality of the upwelling and downwelling events along the coast of Greenland agree with the wind analysis. On average, downwelling events dominate the eastern coast, both in winter and summer, with markedly stronger downwelling events during winter. The southwestern coast is upwelling dominated in winter and downwelling dominated in summer.

Vertical distribution of the tracer on the Greenland shelf clearly demonstrates enhanced wind-driven vertical mixing particularly on the eastern shelf dominated by persistent downwelling-favorable winds all year round. As an example, vertical distribution of the tracer along the Sermilik Trough section is shown in figure 16. In winter (figure 16b), the isolines are vertical indicating homogenously mixed water masses on the shallow part of the shelf. During summer (figure 16a) when the downwelling winds are relaxed, the isolines retreats from the vertical position and are more horizontal. Similar vertical distribution is observed in the simulated S field along the section (Figure 17).

Another mechanism that promotes intense deep mixing of the tracer on the western Greenland shelf is convection during the cold season. Numerical studies by Marson et al. (2017) demonstrated formation of dense water on the west Greenland shelf due to brine rejection. Analysis of the vertical mixing on the Greenland shelf from the 0.08° HYCOM-CICE experiments shows enhanced vertical mixing of the tracer, as well as temperature and salinity, on the western Greenland shelf during winter. Figure 18 shows vertical distribution of S, T, and tracer along the Disco Bay section during February and August 2006. In winter, saline and cold mixed layer is formed in the bay driven by winter cooling and brine rejection. Winter convection mixes surface fresher layers into the deeper layers as demonstrated in the tracer field. During summer, increased freshwater runoff from Greenland and solar radiation forms warm and fresh mixed layer. Stable stratification prevents deep mixing of the tracer (and fresh water) in the bay. Note presence of cold layer below the warm mixed layer and above the warm deep layer. This intermediate layer is the remnant of the winter convection.

In order to demonstrate the impact of Greenland freshwater flux on the near-coastal processes, same section with T, S and tracer fields from the 0.08 HYCOM-CICE without Greenland runoff is presented in Figure 19. In this model experiment, winter convection is deeper and Greenland freshwater vertical mixing is stronger than that in the experiment with Greenland runoff. In summer, the water column is less stable (due to the absence of freshwater flux from the coast) and wind-driven vertical mixing of the tracer is noticeably deeper compared to Figure 18. Note the subsurface cold layer is wider and colder in this model experiment, caused by stronger and deeper winter mixing.

Greenland freshwater spreading in the deep SPNA

Figures 20 and 21 show the spreading of the Greenland freshwater tracer in the North Atlantic simulated in the 0.08° experiment (an animation can be viewed at https://www.youtube.com/watch?v=0nX-mbrg0Co&t=36s).

At every time instance $T = t$, the tracer concentration $C_{tr}(t)$ provides information about the volume of the GFWA at every location in the model domain $\mathcal{D}$. The local tracer mass that relates tracer to the GFWA volume is derived from the simulated C_{tr} as

$$m_{tr}(\mathbf{x}, t) = C_{tr}(\mathbf{x}, t)v(\mathbf{x}, t). \quad (7)$$

The progression of the Greenland tracer spreading in the SPNA (figures 20 and 21) is analyzed in terms of a fraction of the Greenland tracer (k_Ω) accumulated within some control volume $\Omega \subset \mathcal{D}$ defined as

$$k_\Omega(\mathbf{x}, t) = \frac{\int_\Omega C_{tr}(\mathbf{x},t)\, d\mathbf{v}}{\int_\mathcal{D} C_{tr}(\mathbf{x},t)\, d\mathbf{v}} = \frac{m_{tr}(\mathbf{x},t)}{M_{tr}(\mathbf{x},t)} = \frac{\alpha\, v_{Gr}}{\alpha\, V_{Gr}} = \frac{v_{Gr}}{V_{Gr}}, \quad (8)$$

where V_{Gr} is the GFWA defined as

$$V_{Gr}(t) = \int_{t0}^{t} F_{Gr}(T)\, dT, \quad (9)$$

and F_{Gr} is the Greenland freshwater flux anomaly integrated along Greenland coast. Here, the control volume Ω is a grid cell bounded by ocean surface at the top and the geopotential isosurface at some depth.

As follows from Eq. (8), coefficient k_Ω also reflects the fraction of the GFWA accumulated within the control volume Ω (v_{Gr}) to the total GFWA (V_{Gr}) fluxed into the basin. The presented fields of k_Ω in Figures 20 and 21 are derived from the daily mean $C_{tr}(t)$ on July 23 at every year of the simulation (1993–2016) integrated in the upper 50 m and are shown on a natural logarithmic scale.

The Greenland tracer propagates mainly with the boundary currents in agreement with other model studies (e.g., Böning et al., 2016), suggesting that the GFWA generally follows the propagation pathways of the Great Salininty Anomaly (GSA) and other salinity anomalies (Dickson et al., 1988). However, on the southeastern Greenland shelf, the tracer propagates inshore of the East Greenland Current carried by the East Greenland Coastal Current and staying within the shelf break. There is a negligibly small flux of the tracer across the East Greenland Current, which explains the absence of the tracer in the interior Nordic Seas until the tracer is advected into the basin by the North Atlantic current after 12–15 years. After the tracer goes around Cape Farewell,

it is transported north with the West Greenland Current. There is remarkable intensification of the tracer lateral advection to the interior Labrador Sea in the southwest Greenland shelf due to the increased eddy activity along the West Greenland Current. The pathway of the Greenland tracer splits into two major branches at the northern Labrador Sea. One branch follows the continental shelf break turning southwestward with the Labrador Current. The other smaller branch continues along the west coast of Greenland, advecting the tracer into Baffin Bay. The model simulates tracer accumulation over Fylla Bank. Increased concentration of the tracer in the model suggests an elevated concentration of Greenland fresh water in this region. This result concurs with the fact that during the GSA and other salinity anomaly events – which also propagated around Greenland with the EGC and WGC – freshening had strong manifestation over Fylla Bank (Dickson et al., 1988).

Carried by the Labrador Current, the tracer spreads in the Labrador Sea and central North Atlantic. It reaches Newfoundland Island and the Grand Banks within several years, where it mixes with the northward flowing North Atlantic current. Most of the tracer returns into the subpolar basins and some fraction of it flows to the Nordic Seas following the North Atlantic current, in agreement with Cuny et al. (2002). The tracer concentration is more dispersed in the central and eastern North Atlantic. The tracer actively mixes with the ambient waters in the subpolar gyre owing to an increased eddy activity in the region. There is a remarkable difference in terms of the tracer presence in the Nordic Seas and the other subpolar basins. By the end of the simulation (after 24 years), there is >3 times less tracer in the Nordic Seas than in the subpolar gyre. The interior Greenland and Iceland seas remain the local minima with almost no tracer due to cyclonic circulation in the basins, which averts accumulation of the tracer in the interior regions.

Table 1. Freshwater and volume flux estimates in the straits and southeast Greenland shelf from observations (negative fluxes are southward)

Location	Freshwater Flux, mSv (S_{ref})	Volume Flux, Sv	Notes
Nares Strait	-25 ± 12 (34.8)[(a)] -31 ± 4 (34.8)[(b)]	-0.8 ± 0.3[(a)] -0.9 ± 0.1[(b)]	Ship observations, early August 2003
Davis Strait	-93 ± 6 (34.8)[(c)]	-1.6 ± 0.5[(c)]	Moorings, sea gliders, 2004–2010
Denmark Strait	-65 ± 11 (34.8)[(d)] -108 ± 24 EGC and -29 ± 7 separated EGC (34.8)[(e)]	Not measured Overflow water transport 3.4 [(e)]	Mooring observations at the Kogur section, [(d)] August 2011–July 2012 [(e)] 2008, 2011, 2012
Fram Strait	63–95 (34.92)[(f)], 80± 6 (34.92)[(g)] 70±25 (34.9)[(h)]	-2± 2.7[(i)]	[(f)]Hydrographic observations, Aug-Sep 1997, 1998; [(g, i)] Mooring and ship observations along 79ºN; [(h)]Moorings including a Greenland shelf mooring along 78.5ºN
Southeast Greenland shelf	74 ± 12 (34.9)[(j)]	-4.36 ± 0.6 [(j)]	Mooring observations, Overturning in the SPNA, 2014–2016 (~60 ºN, east across the shelf). East Greenland Coastal Current + EGC

[(a)]Munchow et al., 2006
[(b)]Munchow et al., 2007
[(c)]Curry et al., 2014
[(d)]De Steur et al., 2017.
[(e)]Vage et al., 2013.
[(f)]Meredith et al., 2001
[(g)]Rabe et al., 2009;
[(h)]De Steur et al., 2018
[(i)]Schauer et al., 2008
[(j)]Le Bras et al., 2018

References:

Bacon, S., A. Marshall, N. P. Holliday, Y.Aksenov, and S. R. Dye (2014), Seasonal variability of the EastGreenland Coastal Current,J. Geophys.Res. Oceans,119, 3967–3987,doi:10.1002/2013JC009279

Bamber, J., M. van den Boreke, J. Ettema, and J. Lenaerts, 2012. Recent large increase in freshwater fluxes from Greenland into the North Atlantic, Geophys. Res. Lett., 39, L19501, doi:10.1029/2012GL052552.

Bamber, J. L., Tedstone, A. J., King, M. D., Howat, I. M., Enderlin, E. M., van den Broeke, M. R., and Noel, B. (2018), Land Ice Freshwater Budget of the Arctic and North Atlantic Oceans

1. Data, Methods, and Results, Journal of Geophysical Research Oceans, 123(3), 1827-1837, doi:10.1002/2017JC013605.

Bleck, R., C. Rooth, D. Hu, and L.T. Smith (1992), Ventilation patterns and mode water formation in a wind- and thermodynamically driven isopycnic coordinate model of the North Atlantic, J. Phys. Oceanography, 22, 1486-1505.

Böning, C.W., E. Behrens, A. Biastoch, K. Getzlaff, and J.L. Bamber (2016), Emerging impact of Greenland meltwater on deepwater formation in the North Atlantic Ocean. Nat. Geosci. 9, 523–528. doi: 10.1038/ngeo2740.

Cuny, J., P.B. Rhines, P.P. Niiler, and S. Bacon (2002), Labrador Sea boundary currents and the fate of the Irminger Sea Water, JPO, 32, 627-647.

Curry, B., C.M. Lee, B Petrie, R.E. Moritz, and R. Kwok (2014), Multiyear volume, liquid freshwater, and sea ice transport through Davis Strait, 2004–2010, JPO, 44, 1245-1266.

De Steur, L., R. S. Pickart, A. Macrander, K. Våge, B. Harden, S. Jonsson, S. Østerhus, and H. Valdimarsson (2017), Liquid freshwater transport estimates from the East Greenland Current based on continuous measurements north of Denmark Strait, J. Geophys. Res. Oceans, 122, 93–109, doi:10.1002/2016JC012106.

De Steur, L., Peralta-Ferriz, C., & Pavlova, O. (2018). Freshwater export in the East Greenland Current freshens the North Atlantic. Geophysical Research Letters, 45, 13,359–13,366. https://doi.org/10.1029/2018GL080207

Dickson, R. R., J. Meincke, S.-A. Malmberg, and A. J. Lee (1988), The ‘‘Great Salinity Anomaly’’ in the Northern North Atlantic 1968–82, Prog. Oceanogr., 20, 103–151.

Dukhovskoy, D.S., P.G. Myers, G. Platov, M.-L. Timmermans, B. Curry, A. Proshutinsky, J.L. Bamber, E. Chassignet, X. Hu, C.M. Lee, R. Somavilla, 2016. Greenland freshwater pathways in the sub-Arctic Seas from model experiments with passive tracers. J. Geophys. Res. - FAMOS special issue, doi:10.1002/2015JC011290

Fong, D.A., W.R. Geyer (2001), Response of a river plume during an upwelling favorable wind event, JGR-Atmospheres, 106(C1), 1067-1072, doi: 10.1029/2000JC900134.

Havik, L., Vage, K., Pickart, R.S., Harden, B., von Appen, W.-J., Jonsson, S., Osterhus, S. (2017), Structure and variability of the shelfbreak East Greenland Current north of Denmark Strait, JPO, 47, 2631-2646.

Heywood, K.J., McDonagh, E.L., White, M.A. (1994), Eddy kinetic energy of the North Atlantic subpolar gyre from satellite altimetry, JGR, 99(C11), 22,525-22,539.

Jakobsen, P. K., Ribergaard, M. H., Quadfasel, D., Schmith, T., Hughes, C. W. (2003), Near-surface circulation in the northern North Atlantic as inferred from Lagrangian drifters: Variability from the mesoscale to interannual, J. Geophys. Res., 108(C8), 3251, doi:10.1029/2002JC001554, 2003.

Le Bras, I. A.-A., Straneo, F., Holte, J., & Holliday, N. P. (2018). Seasonality of freshwater in the East Greenland Current system from 2014 to 2016. Journal of Geophysical Research: Oceans, 123. https://doi.org/10.1029/2018JC014511

Luo, H., R.M. Castelao, A.K. Rennermalm, M. Tedesco, A. Bracco, P.L. Yager, and T.L. Mote (2016), Oceanic transport of surface meltwater from the southern Greenland ice sheet, Nature Geoscience, 9, 528-532.

Marson, J. M., P. G. Myers, X. Hu,B. Petrie, K. Azetsu-Scott, and C. M. Lee (2017), Cascading off the West Greenland Shelf: A numerical perspective, J. Geophys. Res. Oceans,122, 5316–5328, doi:10.1002/2017JC012801.

Meredith, M.P., Heywood, K.J., Dennis, P.F., Goldson, L.E., White, R.M.P., Fahrbach, E., Schauer, U., Østerhus, S., 2001. Freshwater fluxes through the western Fram Strait. Geophysical Research Letters 28, 1615–1618. doi:10.1029/2000GL011992

Münchow, A., Melling, H., Falkner, K.K. (2006), An observational estimate of volume and freshwater flux leaving the Arctic Ocean through Nares Strait, JPO, 36, 2025–2041.

Münchow, A., K.K. Falkner, and H. Melling (2007), Spatial continuity of measured seawater and tracer fluxes through Nares Strait, a dynamically wide channel bordering the Canadian Archipelago. Journal of Marine Research 65(6):759–788, http://dx.doi.org/10.1357/002224007784219048.

Rabe, B., U. Schauer, A. Mackensen, M. Karcher, E. Hansen, and A. Beszczynska-Möller. 2009. Freshwater components and transports in the Fram Strait: Recent observations and changes since the late 1990s. Ocean Science 5: 219–233, http://dx.doi.org/10.5194/os-5-219-2009

Saha, S., S. Moorthi, H-L Pan, X. Wu, Wang J, Nadiga S, Tripp P, Kistler R, Woollen J, Behringer D, Liu H, Stokes D, Grumbine R, Gayno G, Hou Y-T, Chuang H-Y, Juang H-MH, Sela J, Iredell M, Treadon R, Kleist D, van Delst P, Keyser D, Derber J, Ek M, Meng J, Wei H, Yang R, Lord S, van den Dool H, Kumar A, Wang W, Long C, Chelliah M, Xue Y, Huang B, Schemm J-K, Ebisuzaki W, Lin R, Xie P, Chen M, Zhou S, Higgins W, Zou C-Z, Liu Q, Chen Y, Han Y, Cucurull L, Reynolds RW, Rutledge G, Goldberg M. (2010). The NCEP Climate Forecast System Reanalysis. Bull. Amer. Meteor. Soc., 91, 1015.1057. doi: 10.1175/2010BAMS3001.1

Richardson, P.L. (1983). Eddy kinetic energy in the North Atlantic from surface drifters, JGR, 88, 4355-4367.

Saha, S., S. Moorthi, X. Wu, J. Wang, S. Nadiga, P. Tripp, D. Behringer, Y-T Hou, H-y Chuang, M. Iredell, M. Ek, J. Meng, R. Yang, M. Peña Mendez, H. van den Dool, Q. Zhang, W. Wang, M. Chen, and E. Becker (2014). The NCEP Climate Forecast System Version 2, J. Climate, 27, 2185–2208. doi: http://dx.doi.org/10.1175/JCLI-D-12-00823.1

Schauer, U., A. Beszczynska-Möller, W. Walczowski, E. Fahrbach, J. Piechura, and E. Hansen. 2008. Variation of measured heat flow through the Fram Strait between 1997 and 2006, In: Arctic-Subarctic Ocean Fluxes. R.R. Dickson, J. Meincke, and P. Rhines, eds, Springer, Dordrecht, pp. 65–85.

Vage, K., R.S. Pickart, M.A. Spall, G.W.K. Moore, H. Valdimarsson, D.J. Torres, S.Y. Erofeeva, J.E.O. Nilsen (2013), Revised circulation scheme north of the Denmark Strait, Deep-Sea Research I, 79, 20-39.

Wallcraft, A.J., E.J. Metzger, and S.N. Carroll (2009), Software design description for the HYbrid Coordinate Ocean Model (HYCOM) Version 2.2, Report NRL/MR/7320-09-9166, Naval Research Laboratory, Oceanographic Division, Stennis Space Center, MS 39529-5004, pp. 149.

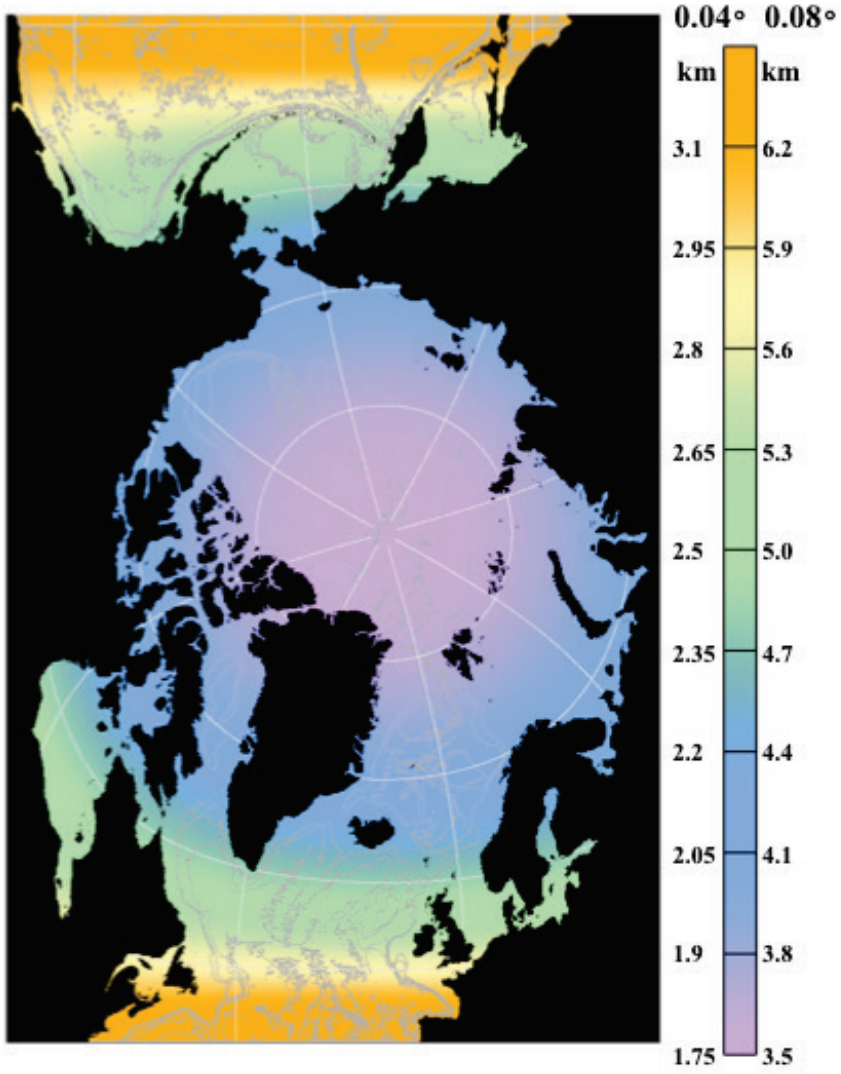

Figure 1. AO HYCOM CICE domain and spatial resolution (km) for 0.08° and 0.04° horizontal grid.

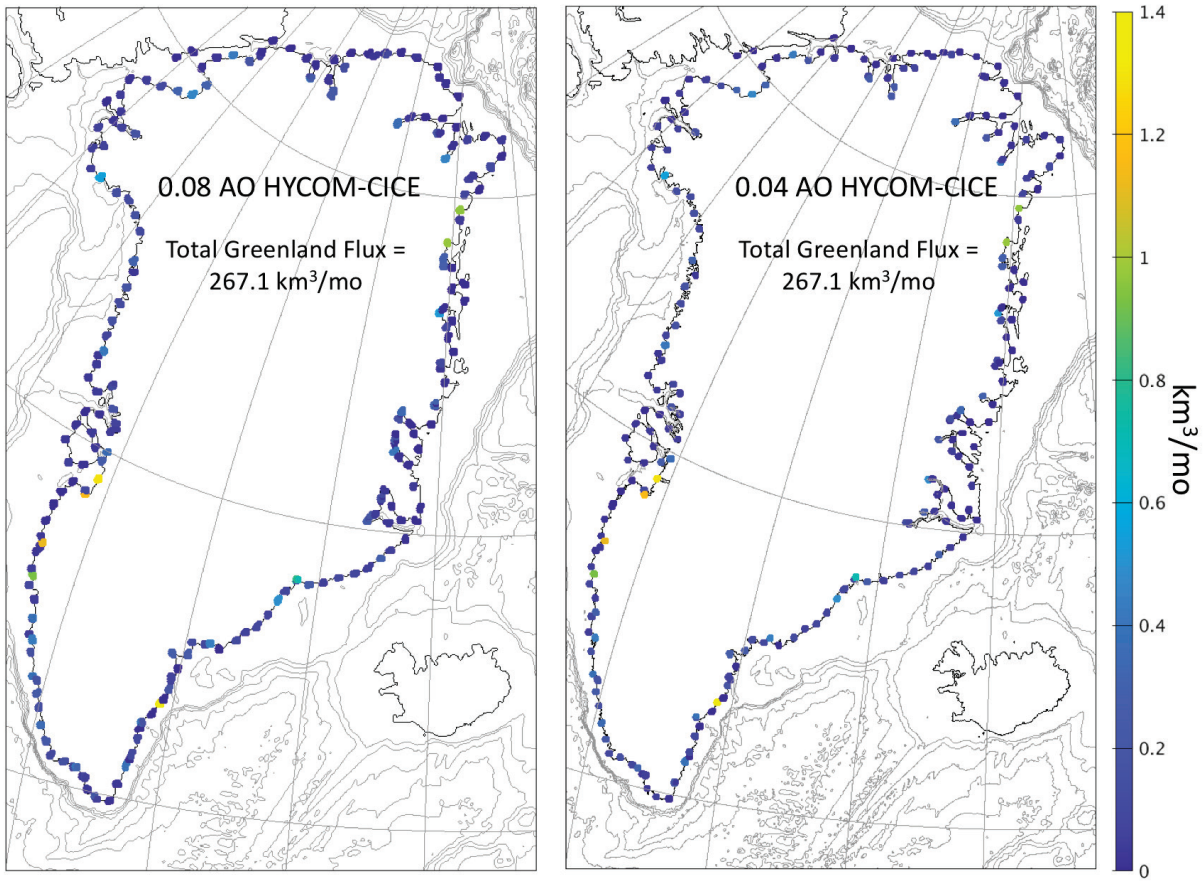

Figure 2. Locations and freshwater fluxes (km3/mo) of Greenland freshwater sources in the 0.08° and 0.04° AO HYCOM-CICE for July 2005.

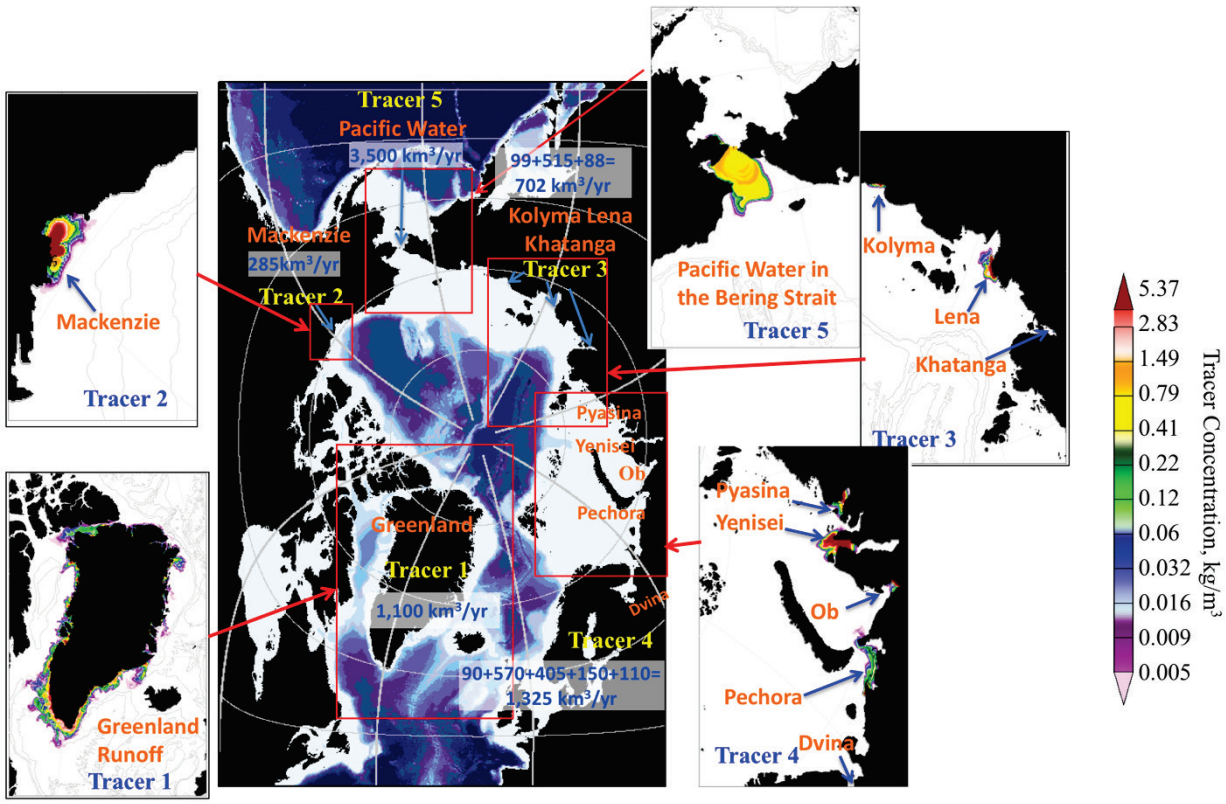

Figure 3. Passive tracer release locations. The colors show tracer concentrations (kg/m3) on a logarithmic scale. The numbers in the map indicate the long-term mean freshwater flux by the sources represented by the individual tracers.

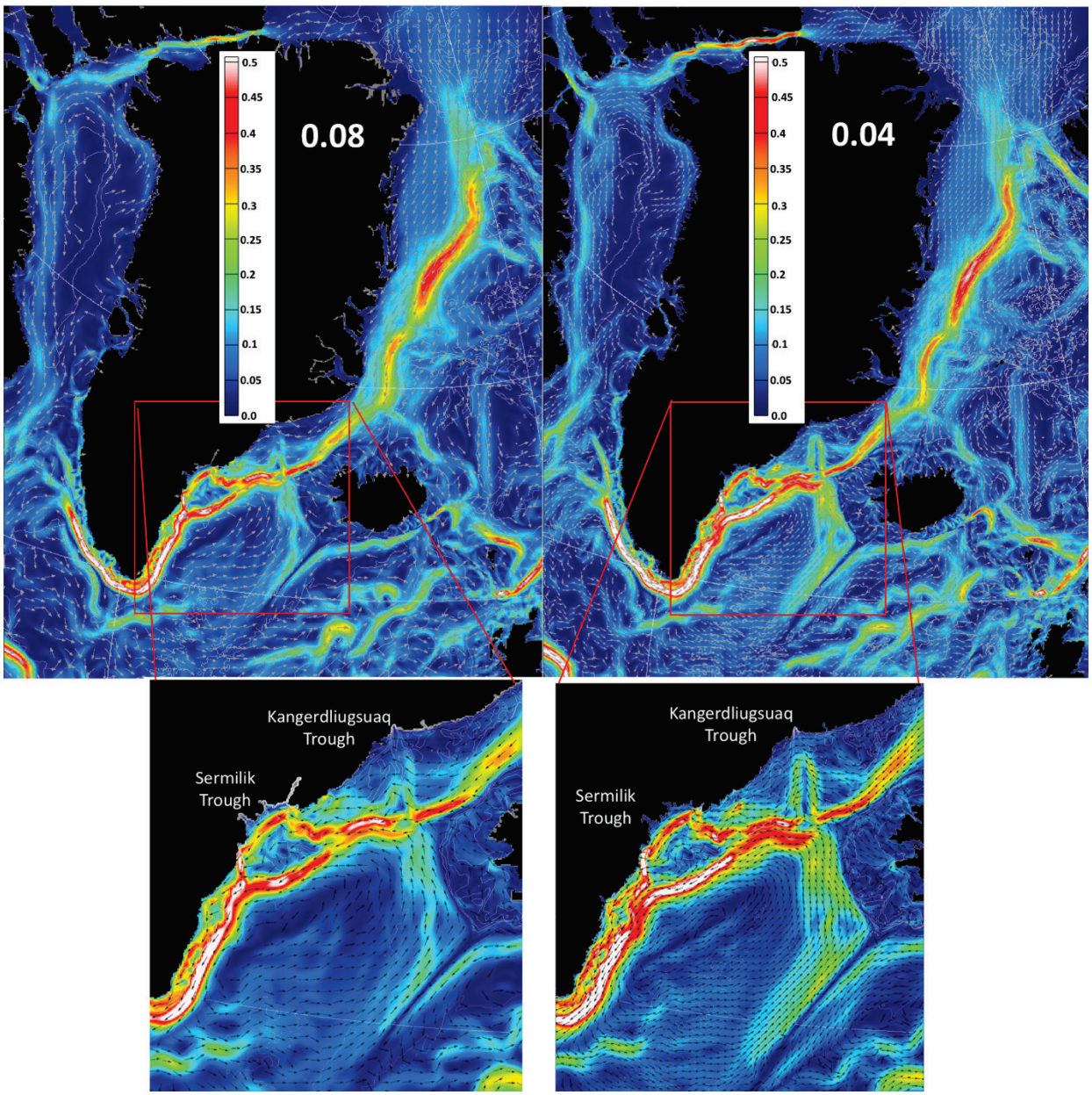

Figure 4. Mean upper 50 m currents (m/s) from the 0.08° and 0.04° HYCOM-CICE.

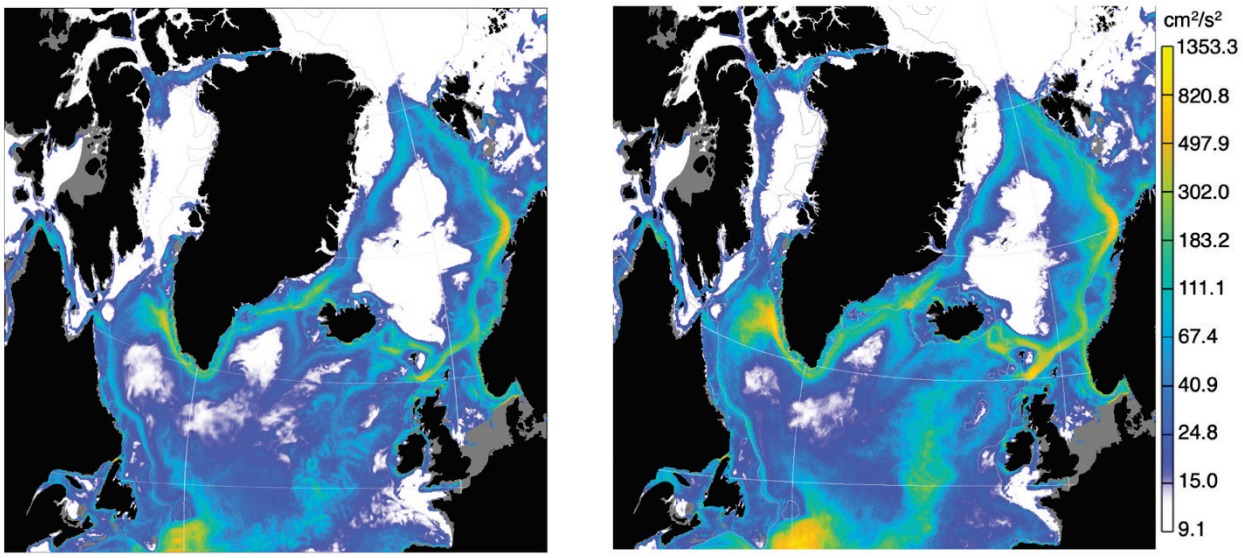

Figure 5. Upper 50 m mean EKE (cm^2/s^2) from the 0.08° and 0.04° HYCOM-CICE.

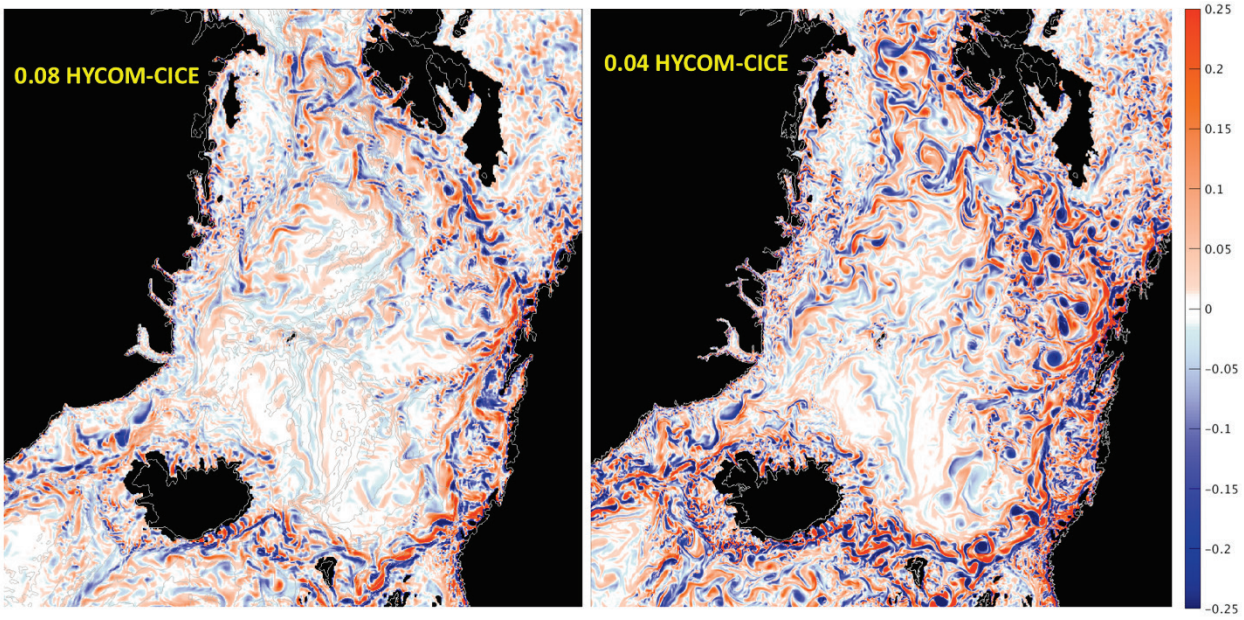

Figure 6. Snapshots of vorticity calculated from the 0.08° and 0.04° HYCOM-CICE velocity fields normalized by the Coriolis parameter. The fields are for January 10, 2006.

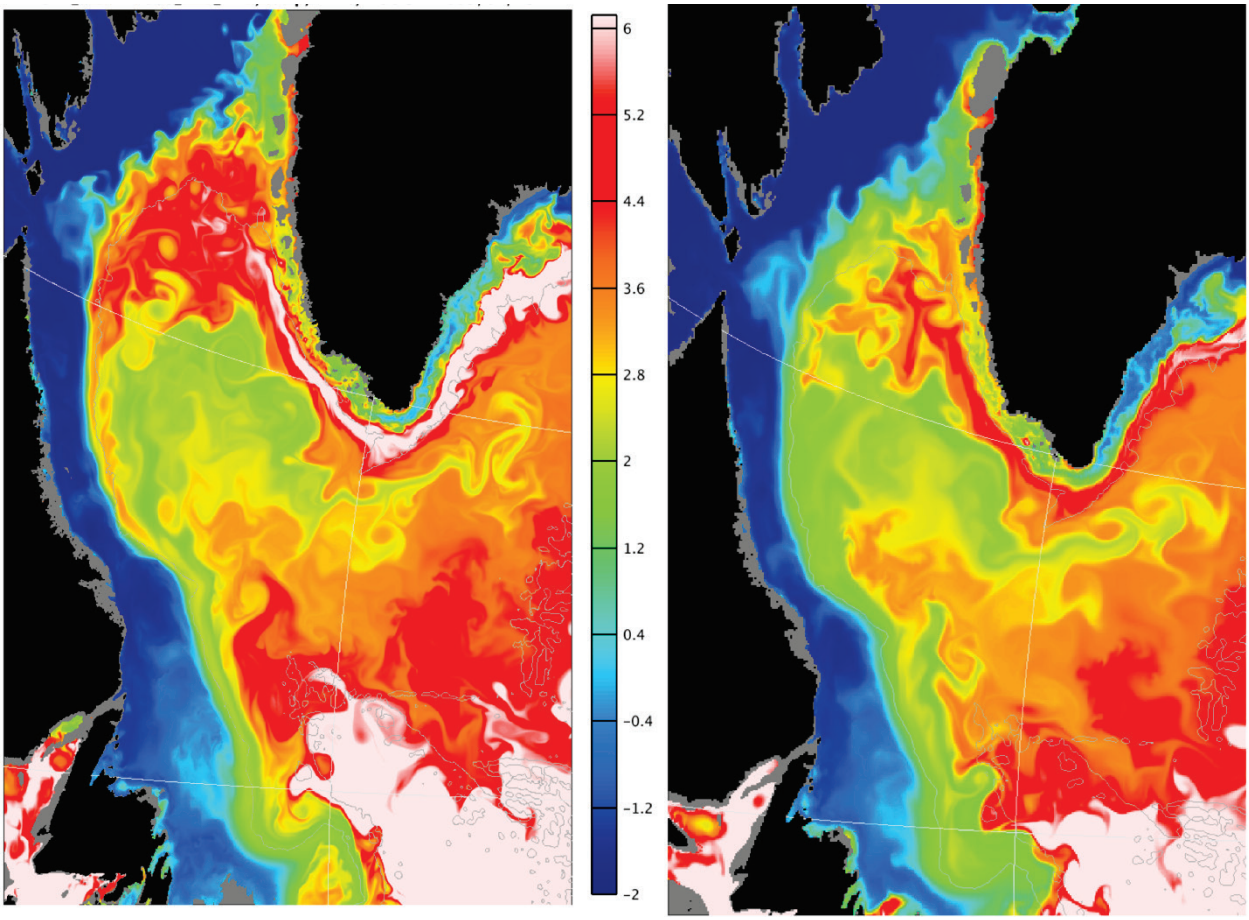

Figure 7. Snapshot of T at 100 m on July 29, 2005 from the 0.04° (left) and 0.08° (right) HYCOM-CICE. The arrows point out the fine structure and eddies represented in the 0.04° HYCOM-CICE that are missing in the 0.08° HYCOM-CICE.

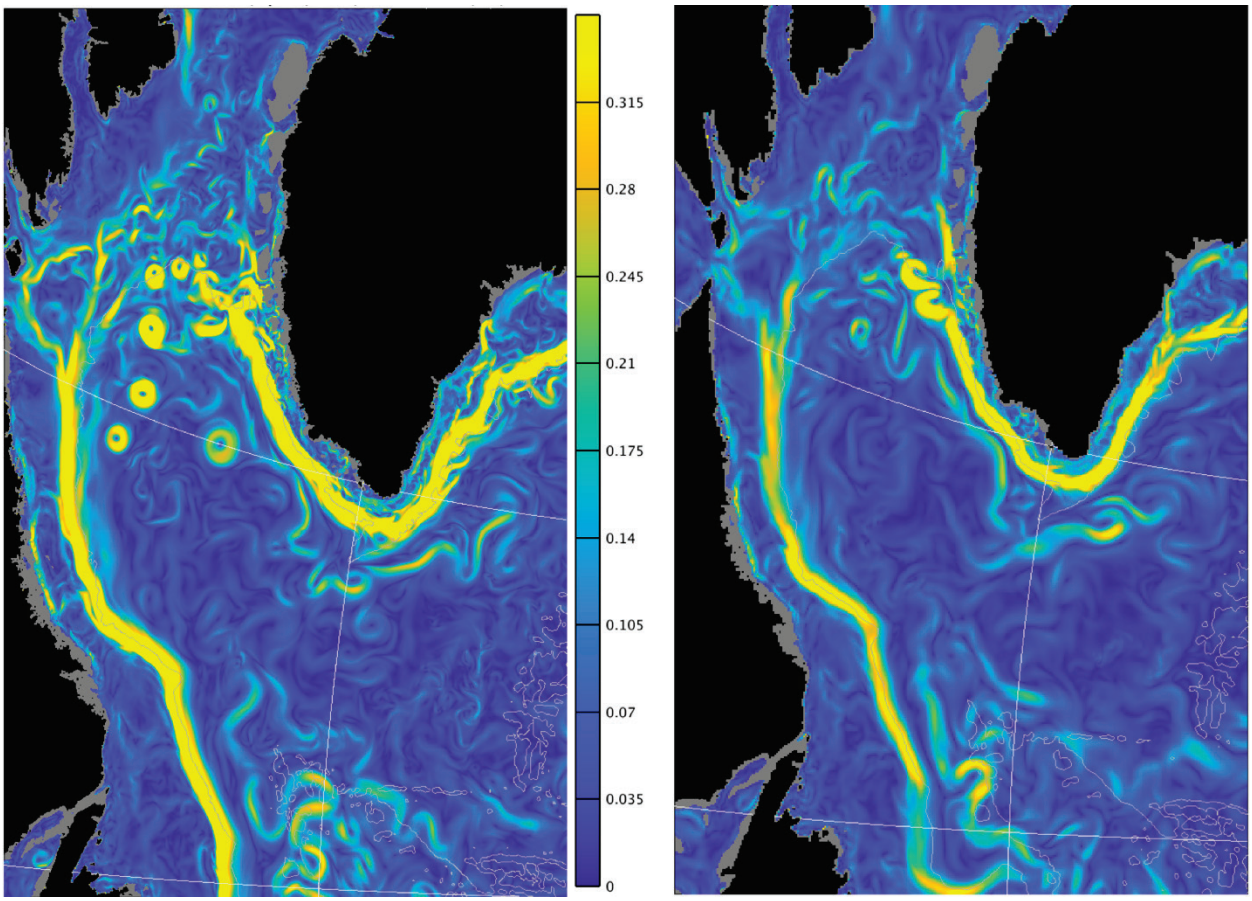

Figure 8. Snapshot of the U field at 100 m on July 29, 2005 from the 0.04° (left) and 0.08° (right) HYCOM-CICE. Colors represent the speed (m/s).

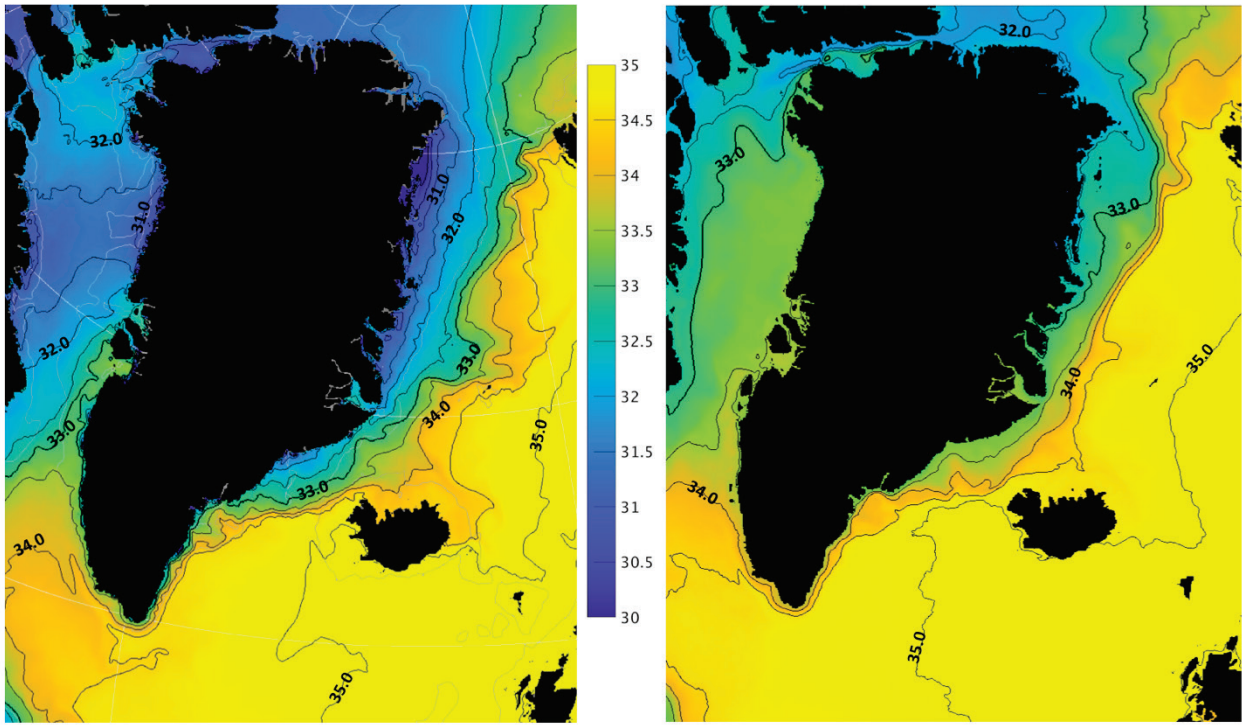

Figure 9. Summer (JJA) mean surface S 2005 from the 0.08° HYCOM-CICE (left) and 0.08° Global HYCOM+NCODA Reanalysis GOFS3.0 (right).

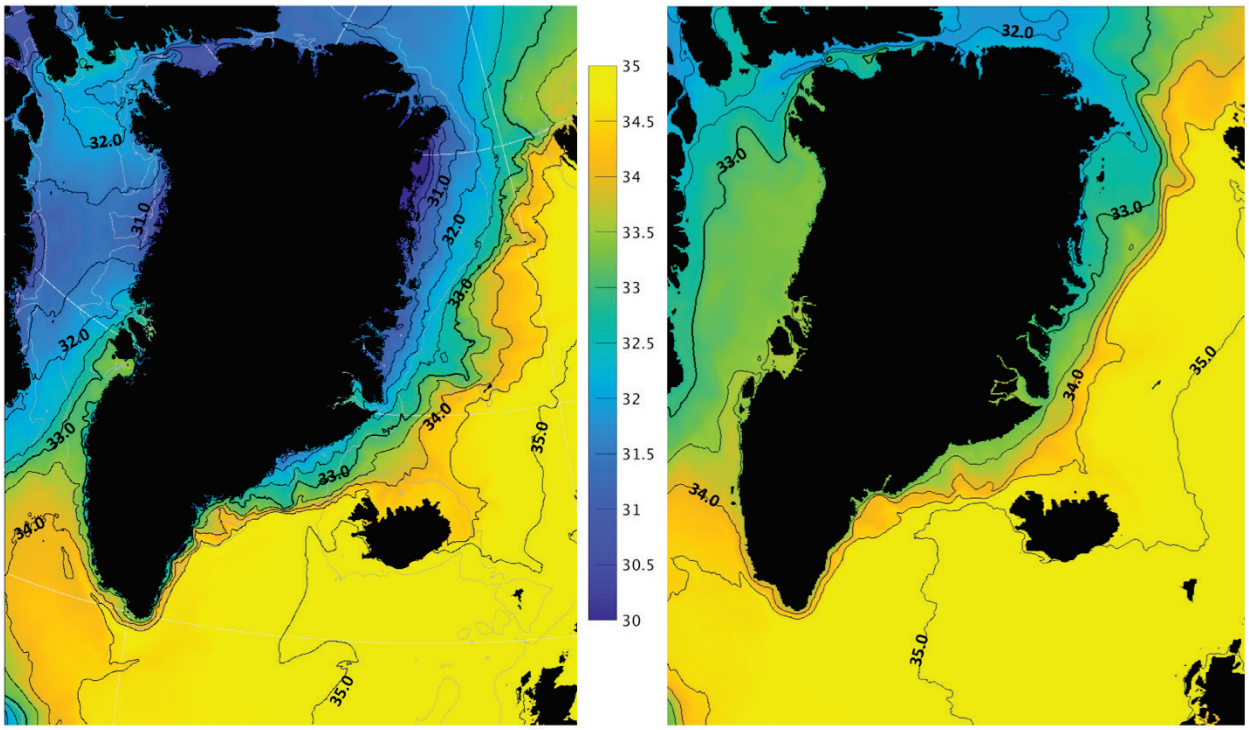

Figure 10. Summer (JJA) mean surface S 2005 from the 0.04° HYCOM-CICE (left) and 0.08° Global HYCOM+NCODA Reanalysis GOFS3.0 (right).

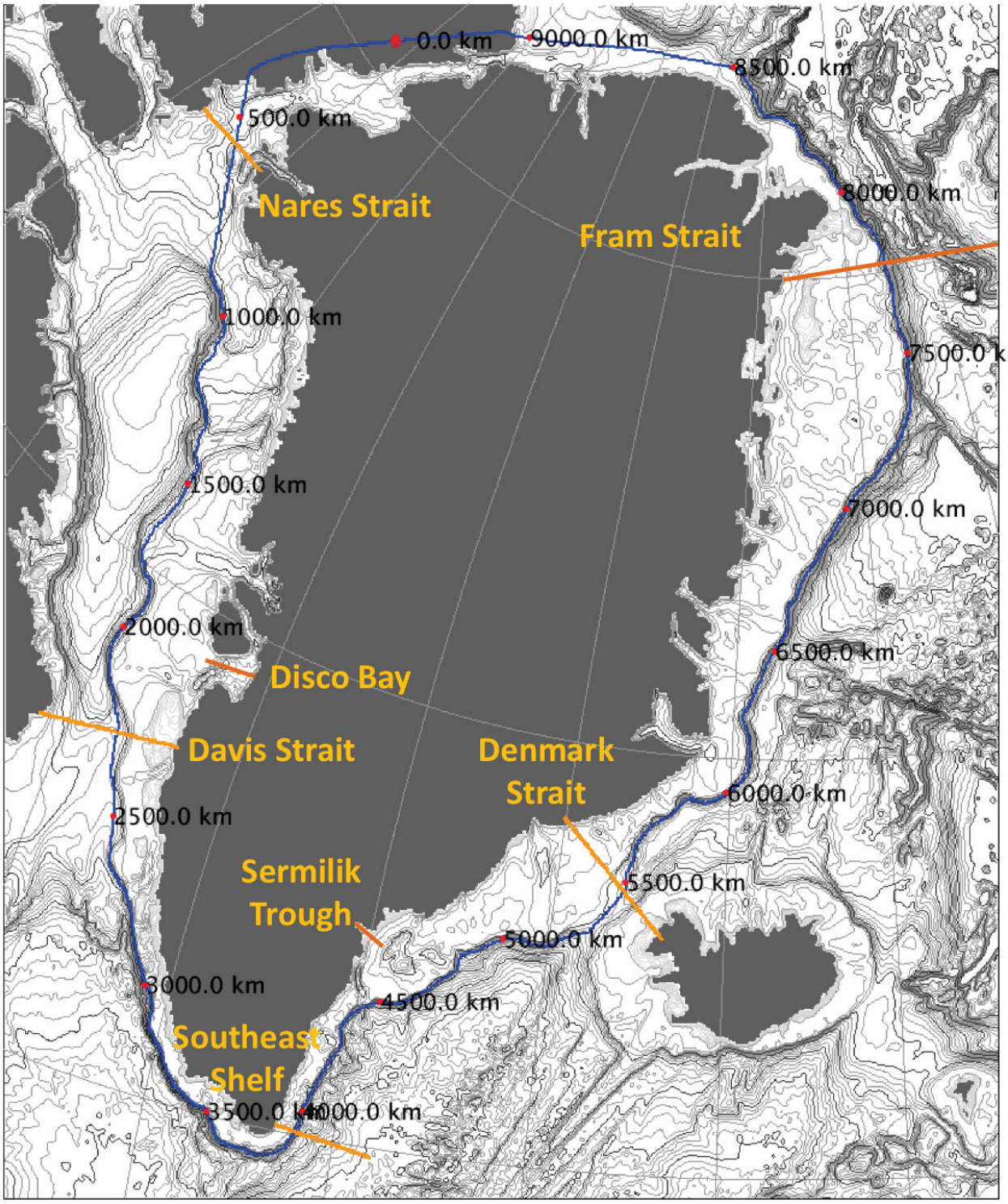

Figure 11. A contour around Greenland (blue) and sections (orange) used for volume, freshwater and heat flux analysis. The contour generally follows the 800-m isobath around Greenland. The numbers on the contour are distances (km).

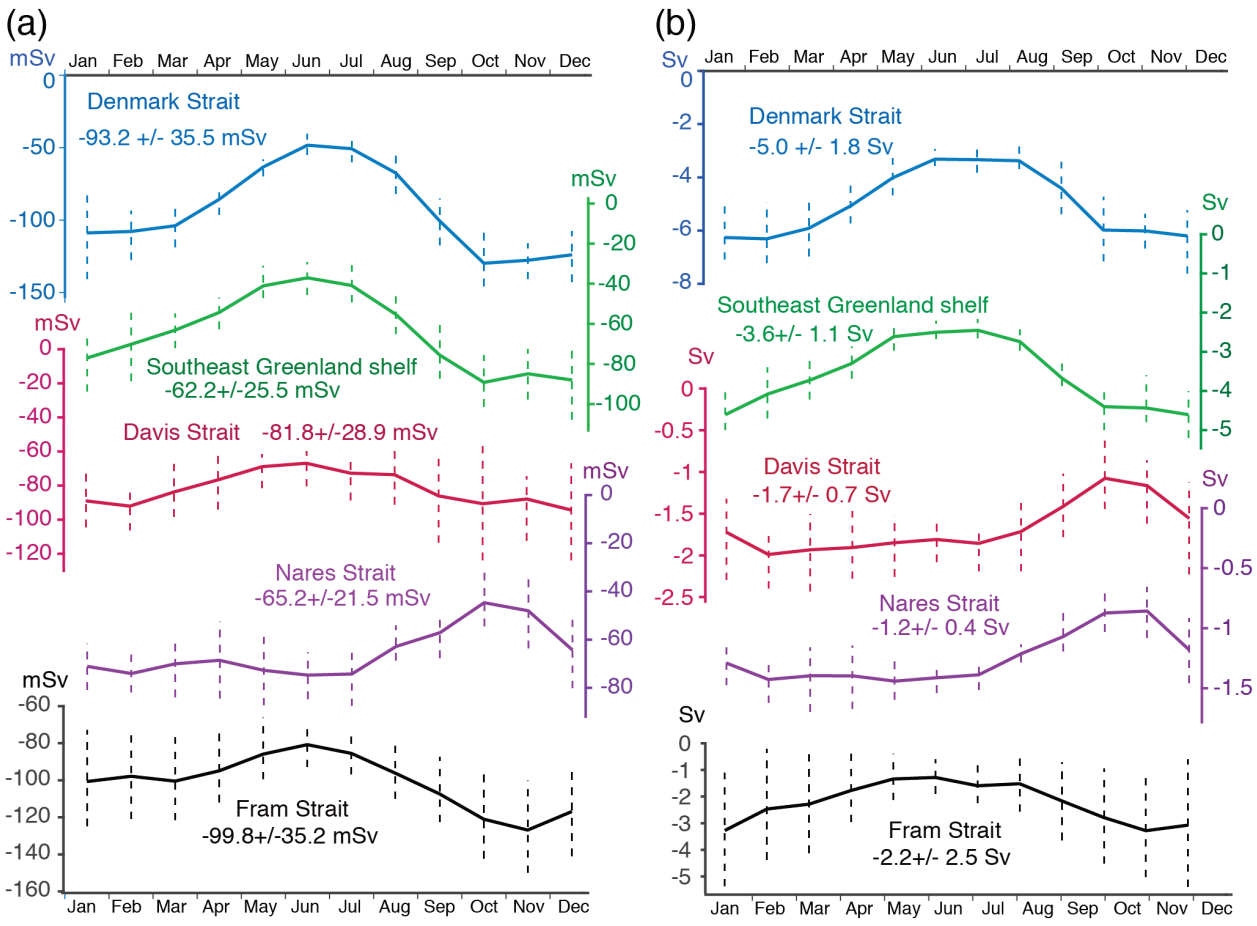

Figure 12. Monthly climatology of freshwater (a) and volume (b) fluxes (mSv and Sv, respectively) from the 0.08° AO HYCOM-CICE. For the freshwater flux is calculated relative to salinity 34.8. The vertical dashed lines range from the 25th to the 75th percentiles.

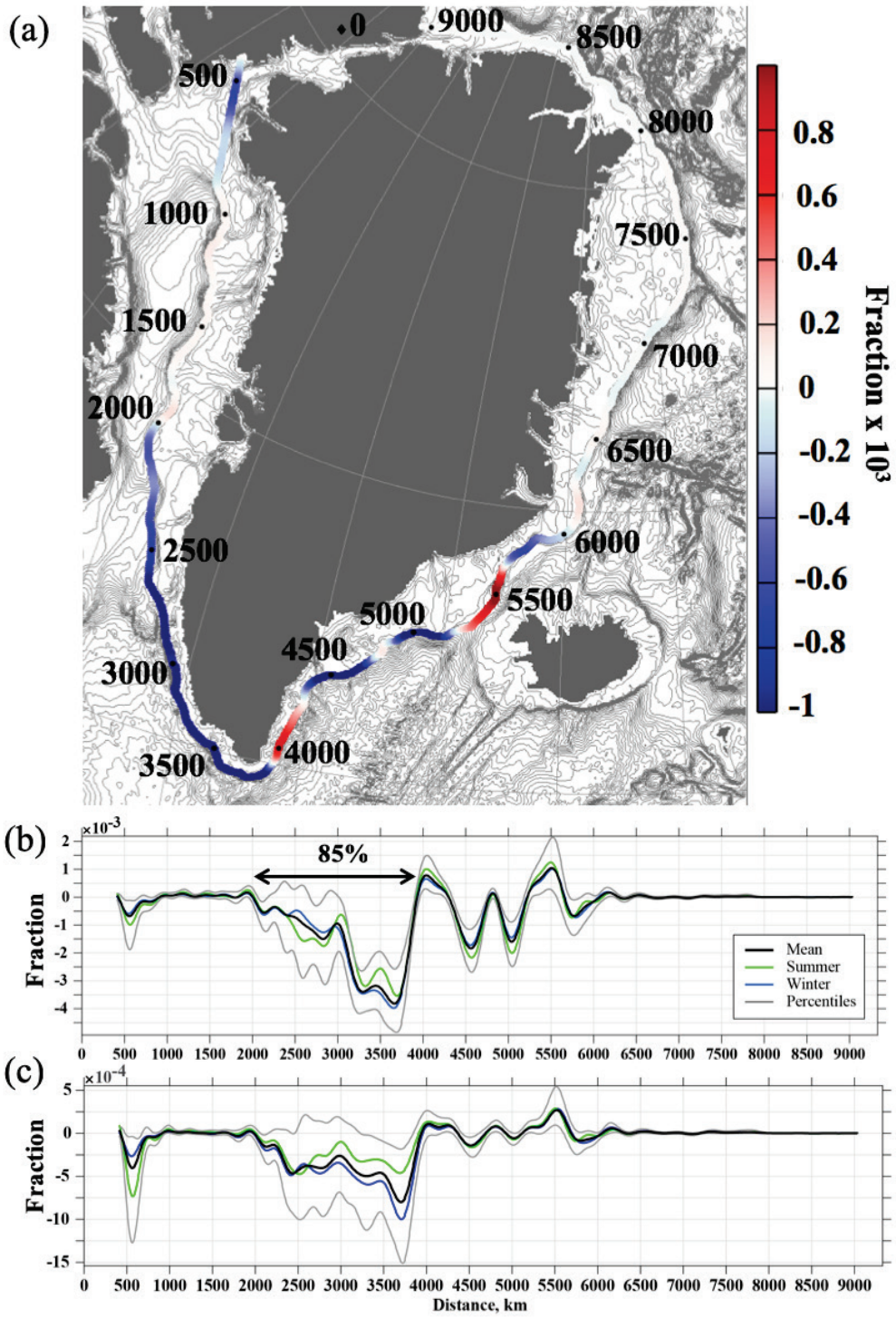

Figure 13. Fraction of the total tracer flux across the contour per 1 km. Negative flux is directed out of the bounded Greenland domain. (a) The map showing the flux across the contour. The contour generally follows the 800 m isobath around Greenland. The numbers on the contour are distances (km). (b) Fraction of the total flux integrated over the whole depth. The arrow depicts the segment of the contour where 85% of the net outflow occurs. (c) Flux integrated over the upper 50 m. In (b) and (c), the blue lines are winter (October–March) and the green lines are summer mean fluxes. The grey lines are the 10th and 90th percentiles.

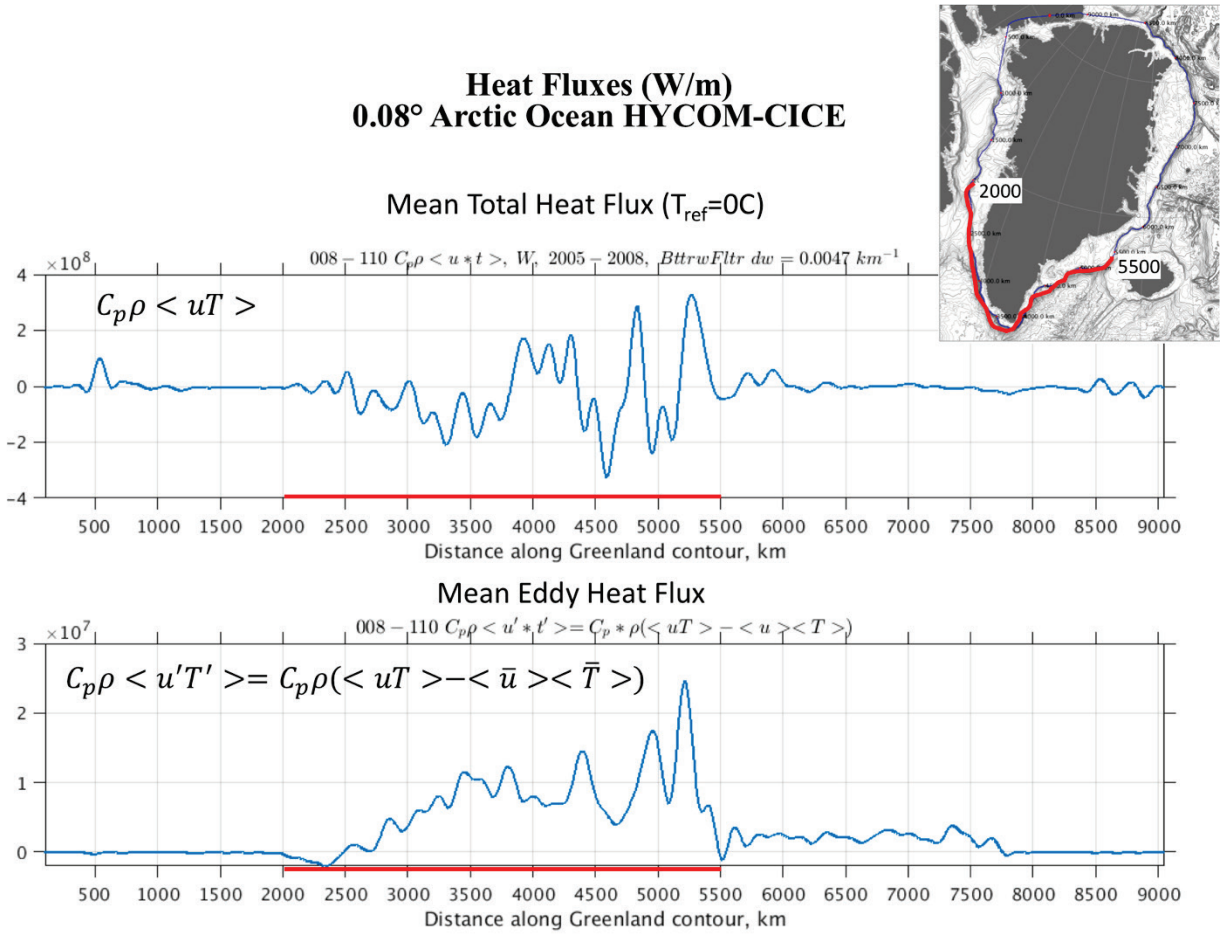

Figure 14. Mean total (top) and eddy (bottom) heat fluxes across the contour. Negative flux is directed out of the bounded Greenland domain. (a) The map showing the flux across the contour. The contour generally follows the 800 m isobath around Greenland. The numbers on the contour are distances (km). (b) Fraction of the total flux integrated over the whole depth. The arrow depicts the segment of the contour where 85% of the net outflow occurs. (c) Flux integrated over the upper 50 m. In (b) and (c), the blue lines are winter (October–March) and the green lines are summer mean fluxes. The grey lines are the 10th and 90th percentiles.

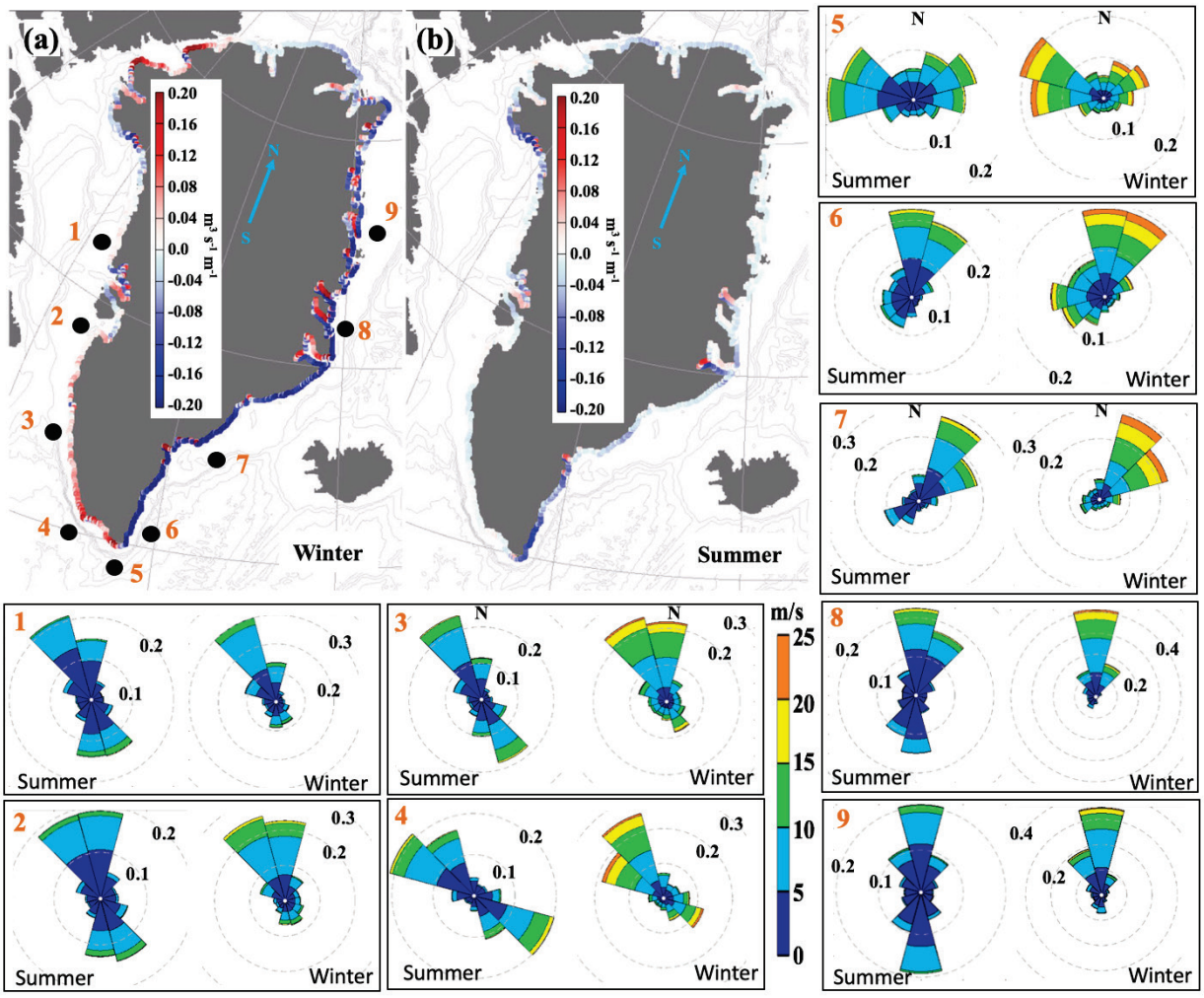

Figure 15. The maps in (a) and (b) show the upwelling index (m^3 s^{-1} per 1 m of the coast line) during winter (a) and summer (b) over 1997–2016. The transport is estimated from the CFSR and CFSv2 surface winds. The black dots in (a) and the numbers designate locations for which the wind rose diagrams are presented. In the wind rose diagrams, colors indicate the wind speed (m s^{-1}) and the dashed circles are occurrences of winds from the binned directions. Note the difference in orientation of the north in the wind roses and the maps.

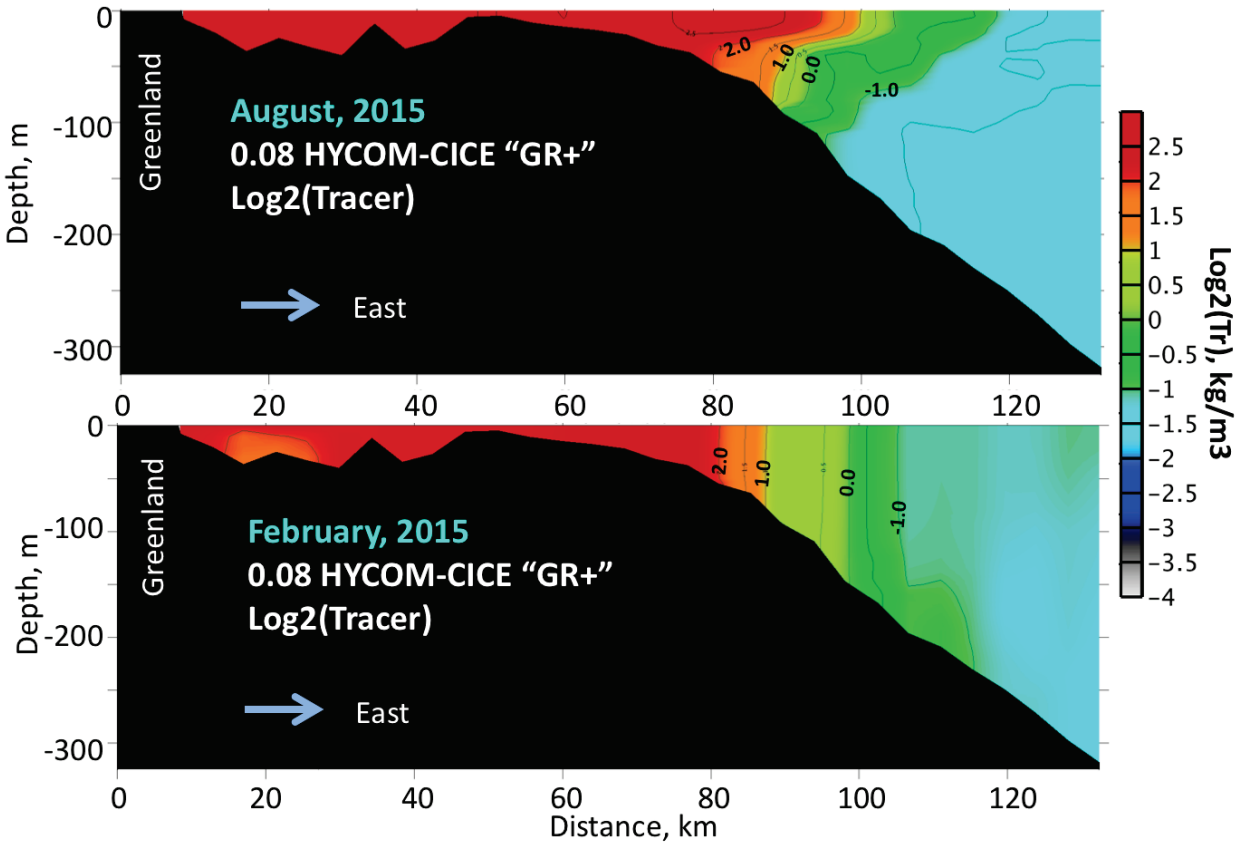

Figure 16. Vertical distribution of the passive tracer concentration from the 0.08° HYCOM-CICE along the Sermilik Trough section in August and February, 2015. The concentration is in the logarithmic scale.

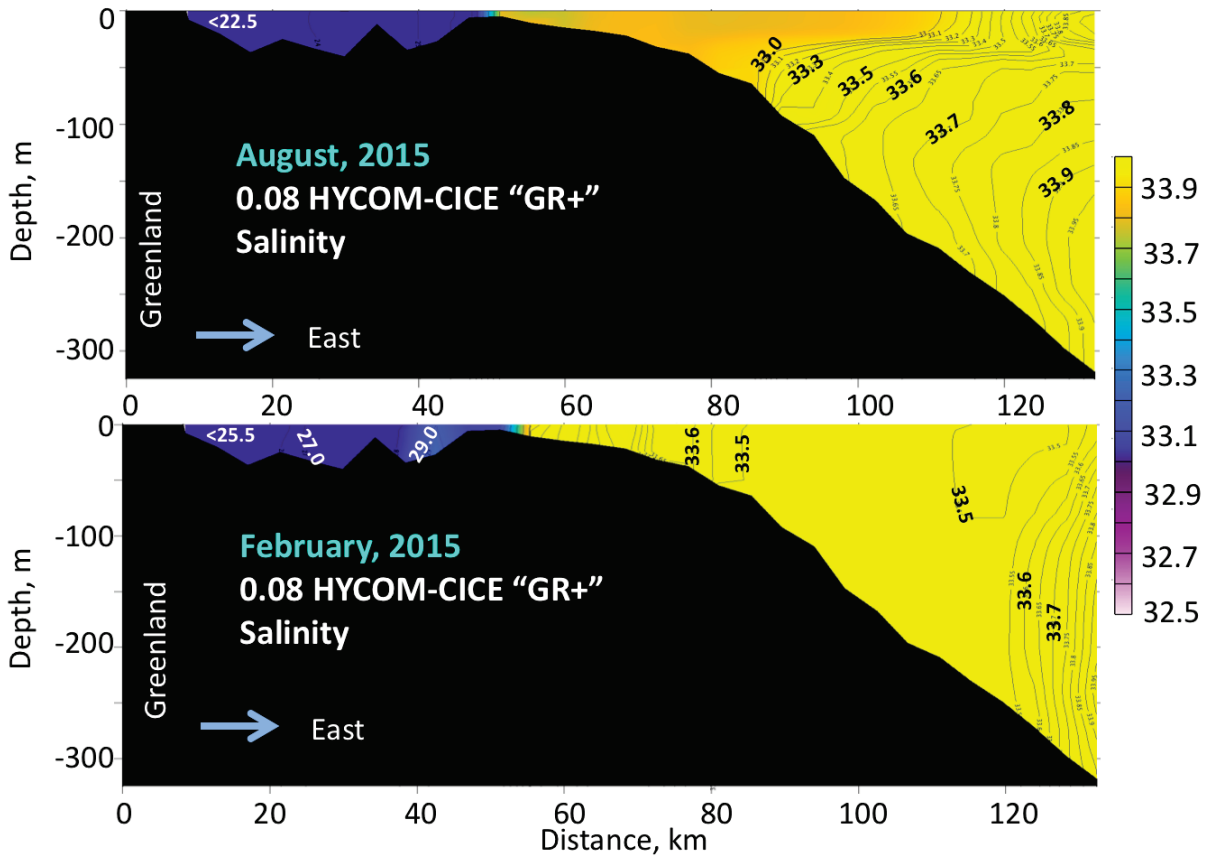

Figure 17. Vertical distribution of salinity from the 0.08° HYCOM-CICE along the Sermilik Trough section in August and February, 2015.

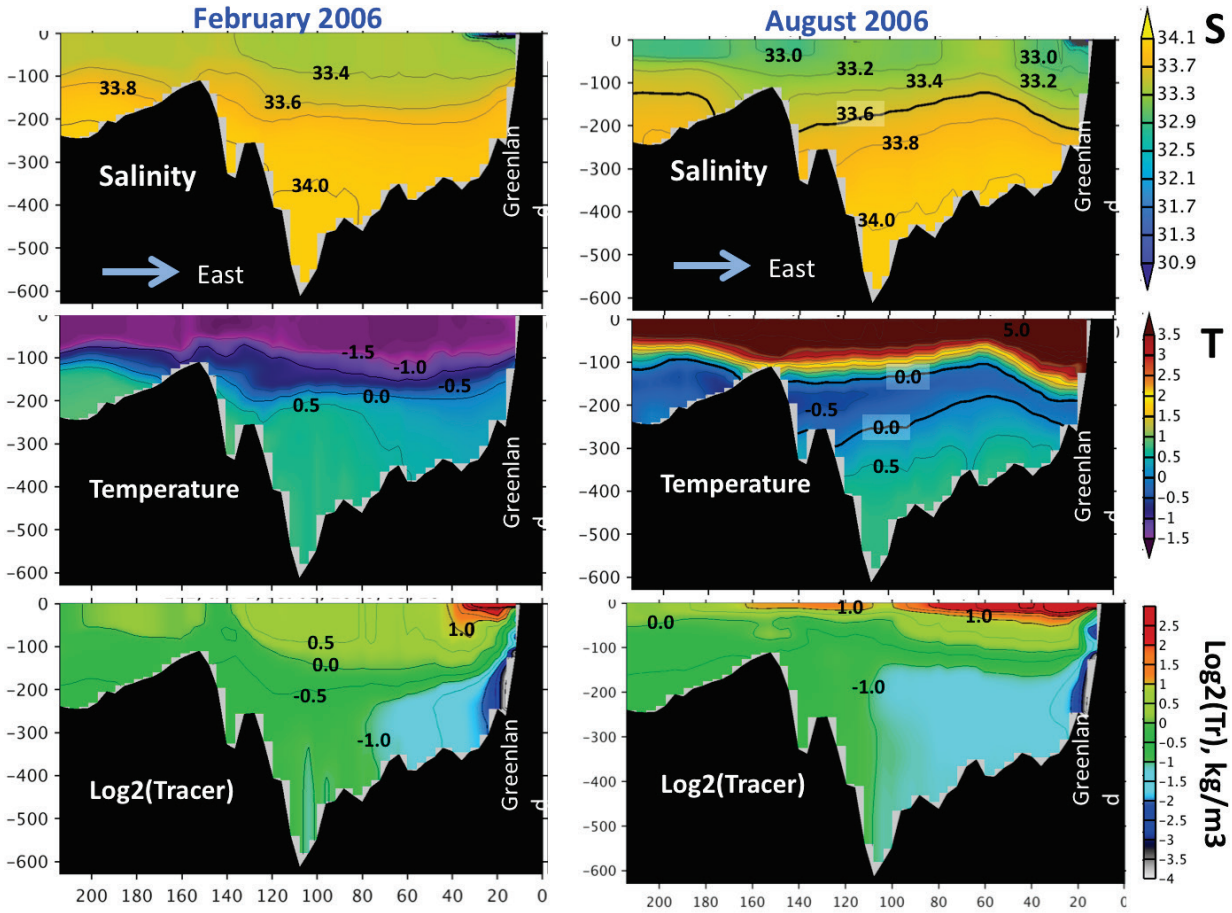

Figure 18. Vertical distribution of S (top), T (middle), and tracer concentration (log scale, bottom) from the 0.08° HYCOM-CICE along the Disco Bay section in February (left column) and August (right), 2006.

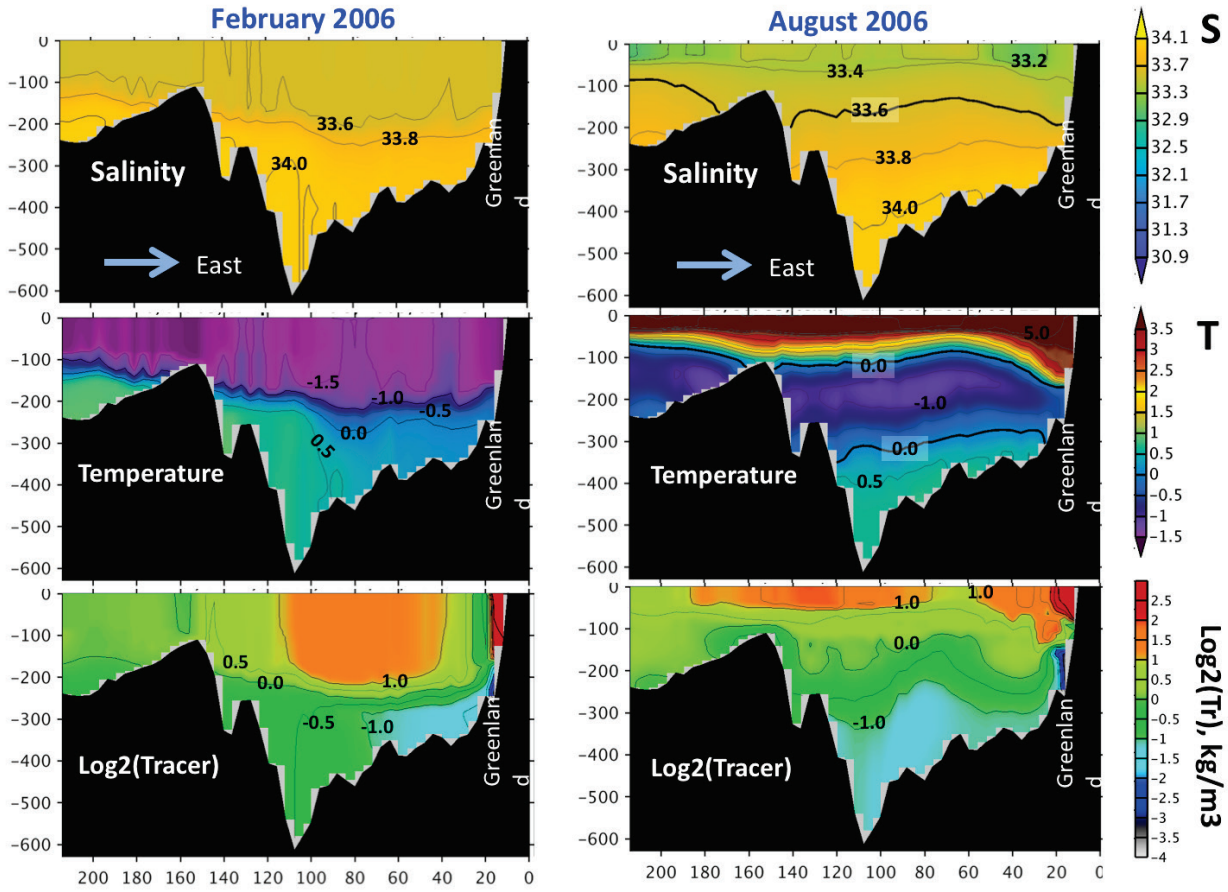

Figure 19. Same as figure 18 but from the 0.08° HYCOM-CICE without Greenland runoff.

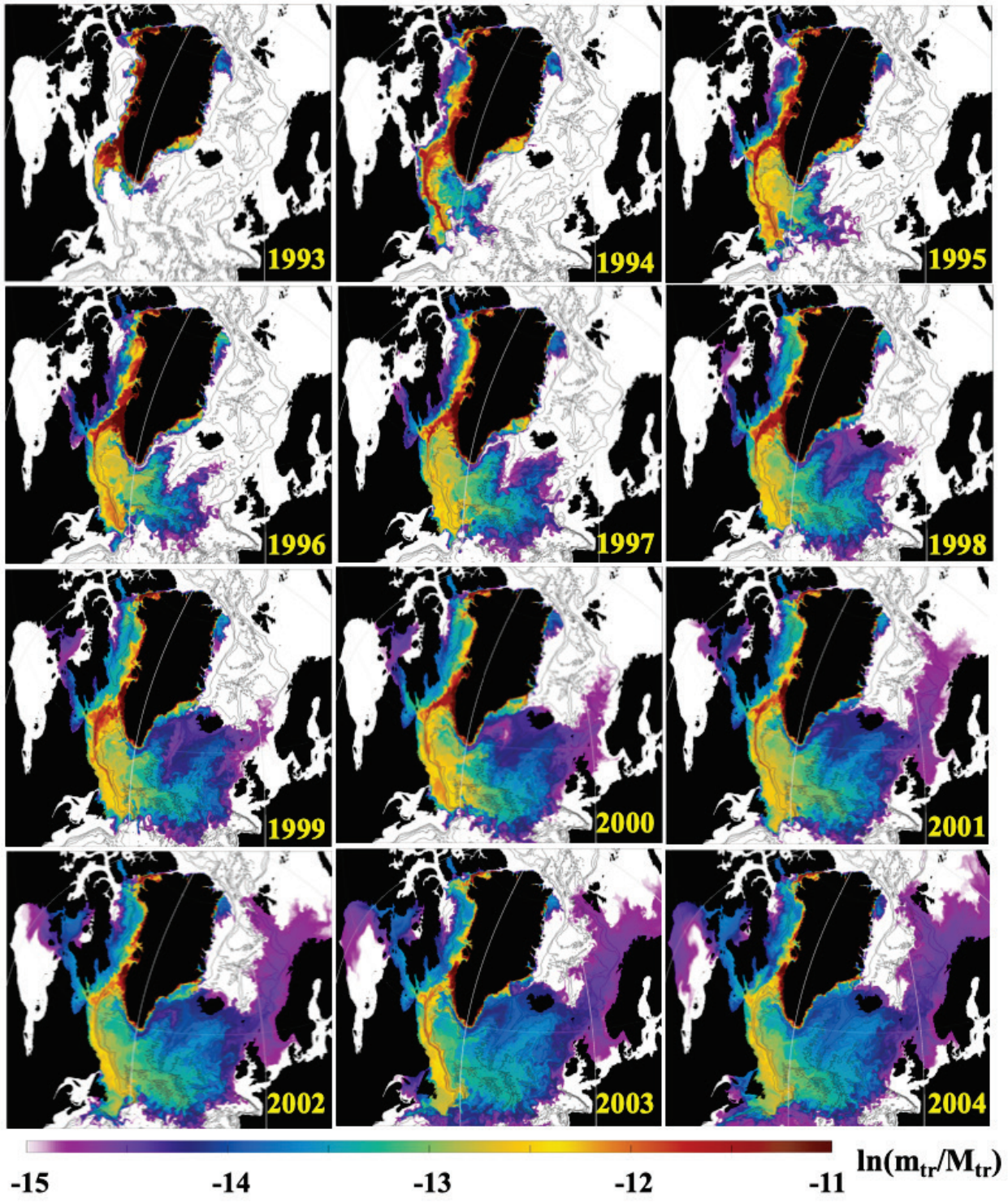

Figure 20. Snapshots of ln($k\Omega$) (Eq. (2)) derived from the daily mean tracer concentration in the upper 50 m from 0.08° AO HYCOM-CICE during 1993–2004. The coefficient is given on a natural logarithmic scale. Each snapshot is for July 23.

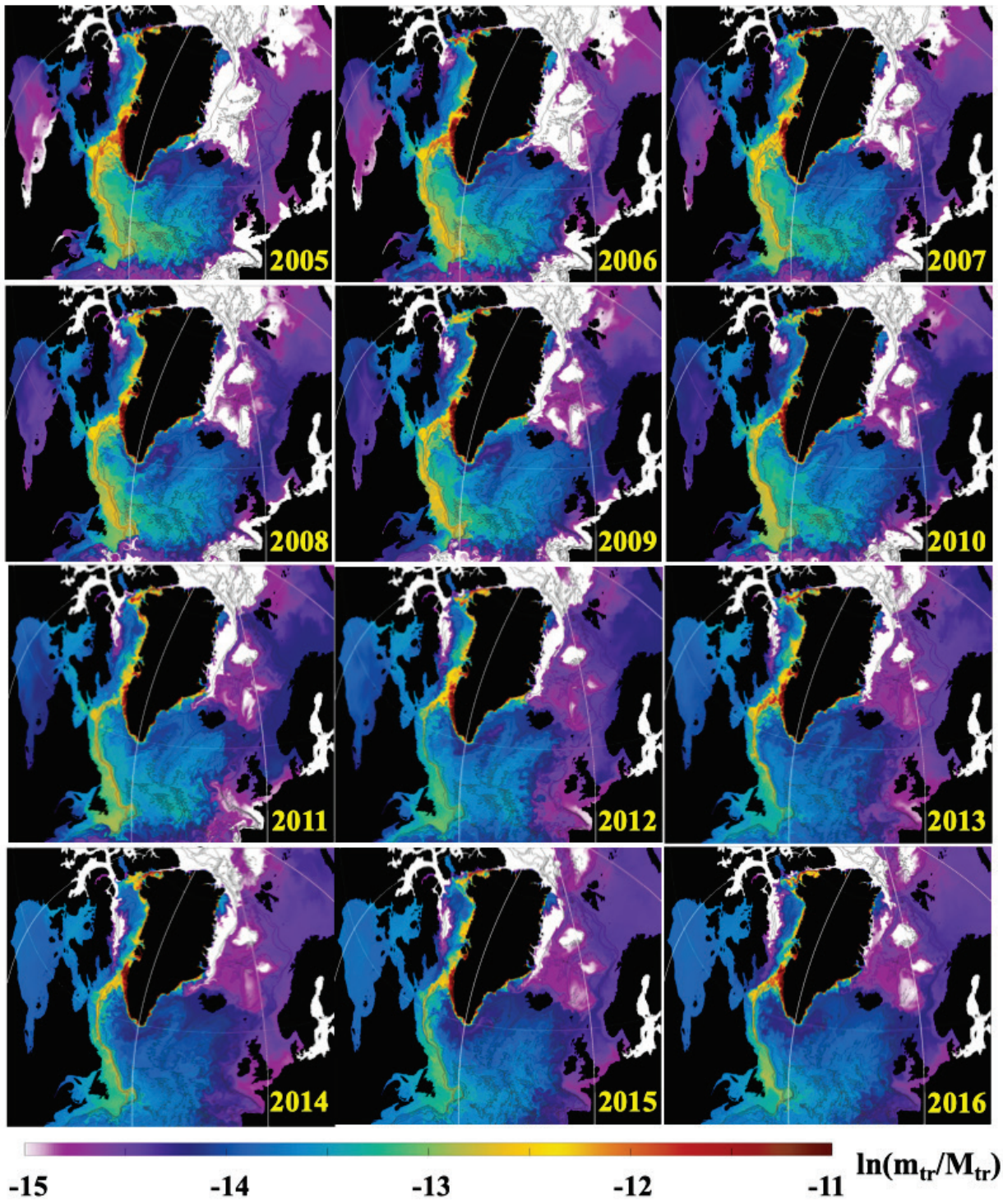

Figure 21. Snapshots of ln(k_Ω) (Eq. (2)) derived from the daily mean tracer concentration in the upper 50 m from 0.08° AO HYCOM-CICE during 2005–2016. The coefficient is given on a natural logarithmic scale. Each snapshot is for July 23.